

Computational Analysis of Binding Interactions between Novel Boronic Acid Derivatives and Urokinase Type Plasminogen Activator (uPA)



By

Syeda Mashaal Shah

(Fall 2017-MS BI-2 00000203721)

(MS Bioinformatics)

Supervised by:

Dr. Mehak Rafiq

Research Centre for Modelling and Simulation

National University of Sciences and Technology

Islamabad, Pakistan.

May 2020

Computational Analysis of Binding Interactions between Novel Boronic Acid Derivatives and Urokinase Type Plasminogen Activator (uPA)

A thesis submitted in partial fulfilment of the requirement for the degree of
Master's in bioinformatics



By

Syeda Mashaal Shah

(Fall 2017-MS BI-2 00000203721)

Supervised by:

Dr. Mehak Rafiq

Research Centre for Modelling and Simulation

National University of Sciences and Technology

Islamabad, Pakistan.

May 2020

Dedication

I dedicate this work to my beloved parents and my supervisor as a token of affection and gratitude who had faith in me and taught me great virtues that encouraged me to work with positive attitude and patience in my life with passion.

Certificate of Originality

I hereby declare that the results presented in this research work titled as “Computational Analysis of Binding Interactions between Novel Boronic Acid Derivatives and Urokinase Type Plasminogen Activator (uPA)” are generated by myself. Moreover, none of its contents are plagiarized nor set forth for any kind of evaluation or higher education purposes. I have acknowledged/referenced all the literary content used for support in this research work.

Syeda Mashaal Shah

Fall 2017-MS BI-2 00000203721

Acknowledgement

All the praises be to Almighty Allah the most compassionate and the most merciful, who has bestowed upon me the power and ability to think and grow, empowering me to play my role in conveying a little share of my knowledge. I will forever be grateful to my dear father and loving mother who helped me get through my research phase and for their love and emotional support, for always encouraging me to keep going no matter what. Moreover, I would like to add, I would not have accomplished what I have without the constant support of my generous supervisor Dr. Mehak Rafiq on whom I relied for guidance and help at any time. I am much obliged to my guidance committee members Dr. Rehan Paracha and Dr. Uzma Habib who have always been available for their humble assistance at various stages of my study and provided me with their valuable feedback and opinion.

Contents

Acknowledgment	Error! Bookmark not defined.
Contents	ii
List of Abbreviations	vi
List of Figures	viii
List of Tables	xii
Abstract	xiii
1 Introduction.....	1
1.1 Cancer.....	1
1.2 Serine proteases.....	2
1.3 Urokinase-type plasminogen activator receptor system (uPAR)	3
1.4 Boronic Acid	6
1.4.1 Derivatives of Boronic acids as protease inhibitors.....	7
1.5 Computational techniques applied	8
1.5.1 Structure based drug design (SBDD).....	9
1.5.2 Ligand based drug design (LBDD).....	9
1.5.3 Quantum mechanical methods (QM).....	10
1.6 Objectives.....	13

2	Literature Review.....	14
2.1	Role of uPA and uPAR in cancer.....	15
2.2	Inhibitors developed against uPA	17
2.3	Cutting-edge techniques used for finding effective inhibitors for uPA	21
2.3.1	Structure Based studies for uPA	21
2.3.2	Ligand Based studies for uPA.....	25
2.3.3	Quantum mechanical studies for uPA.....	27
3	Methodology.....	30
3.1	Protein binding pocket prediction	31
3.2	Retrieval of crystal structure	31
3.3	uPA binding pocket prediction.....	32
3.3.1	DoGsite Scorer.....	32
3.3.2	RaptorX.....	33
3.4	Docking	33
3.4.1	Molecular operating environment (MOE)	34
3.4.2	Genetic optimization and ligand binding (GOLD)	35
3.5	Active site extraction/Model	35
3.6	Pharmacophore model.....	35

3.7	Quantum mechanical studies/calculations	36
3.7.1	Gaussian 09 and Gauss view.....	36
3.7.2	Density functional theory (DFT) method Density	36
3.7.3	Geometry Optimization/Energy Optimization.....	36
3.7.4	Frequency Calculation	37
3.7.5	Single point Energy and Self-Consistent Reaction Field Calculation	37
3.8	MOLDEN.....	37
4	Results and Discussion	Error! Bookmark not defined.
4.1	Molecular docking.....	Error! Bookmark not defined.
4.2	Binding pocket prediction	39
4.2.1	DoGsite scorer	39
4.2.2	Results from RaptorX	42
4.2.3	Analysis of generated pockets	43
4.3	Molecular Docking.....	44
4.3.1	MOE Results.....	44
4.3.2	GOLD Results.....	50
4.3.3	Validation and accuracy.....	56
4.3.4	Pharmacophore modeling	59

4.3.5	Template selection	59
4.3.6	Selection of test set and activity Cut-off.....	60
4.3.7	Query generation.....	60
4.3.8	Model evaluation	61
4.3.9	Model extraction	63
4.4	Quantum mechanical studies.....	Error! Bookmark not defined.
4.4.1	Ligand-protein complex geometry optimization	64
4.4.2	Binding pocket geometry optimization.....	65
4.4.3	Ligand Geometry optimization	66
4.4.4	Frequency calculation for all optimized geometries	67
4.4.5	Single point energy calculation for all optimized geometries	67
5	Conclusion	69
	References.....	71

List of Abbreviations

ECM	Extracellular matrix
PA system	Plasminogen activator (PA) system
uPA	Urokinase-type plasminogen activator system
MOE	Molecular operating environment
GOLD	Genetic optimizations and ligand binding
CAFs	Cancer-associated fibroblasts
PDB	Protein Data Bank
	Urokinase-type plasminogen activator receptor
uPA	system
PAI-1	plasminogen activator inhibitor-1
PAI-2	Plasminogen activator inhibitor-2
GPI	Glycophosphatidylinositol
MMP	Matrix metalloproteases
LD50	Median lethal dosage
HMA	Hexamethylene amiloride
FDA	Food and Drug Administration
CADD	Computer aided drug design
QM	Quantum Mechanical
DFT	Density Functional Theory
SAR	Structure-activity relationship
NMR	Nuclear magnetic resonance
SBDD	Structure based drug design
LBDD	Ligand based drug design
MD	Molecular Dynamics
SBVS	Structure based virtual screening
QSAR	Quantitative structure activity relationship
MM	Molecular Mechanics
IUPAC	International Union of Pure and Applied Chemistry

SCRF	Self-consistent reaction fields
BM	Basement membrane
IHC	Immunohistochemistry
RMSD	Root mean square deviation
NCI	National cancer institute
SVM	Support Vector Machines
CPCM	Conductor like polarizable continuum method
3D	3 dimensional
MCC	Matthews correlation coefficient

List of Figures

Figure 1.1 Presentation of steps involved in a metastatic cascade [3].....	2
Figure 1.2 Urokinase type plasminogen activation system in action.....	4
Figure 1.3 Borinic and boronic acids are organoboron species derived from borane	7
Figure 2.1 Compound 15	18
Figure 2.2 A. Quercetin bound to the binding pocket of uPA. B. Electron density map around Quercetin molecule as magenta web. C. Asp189 residue depicted in stick form at the bottom of S1 binding site shown from side view with electrostatic potential surface. D. Top view of the binding pocket. E. Interacting amino acids in the S2 pocket	19
Figure 2.3 Schematic representation of the domain structure of pro-uPA and uPA. The two-chain, active form of uPA is generated from the single-chain precursor form (pro-uPA) by plasmin-mediated cleavage of the Lys158-Ile159 peptide bond. The active form of uPA is	22
Figure 2.4 Functional process chart of structure-based drug design (SBDD)	25
Figure 3.1 Work flow representing the steps followed to obtain the objectives of this study.	31
Figure 3.2 Web-Server-GUI present for DoGsite scorer for the prediction of binding sites of different proteins.....	32
Figure 3.3 Main server of RaptorX for protein structure prediction.....	33
Figure 3.4 A workflow for structure based studies involving data collection and protein ligand prepared followed by docking, pose generation for each ligand and pose evaluation	34

Figure 4.1 Results generated by DoGsite scorer showing nine possible binding pockets	Error! Bookmark not defined.
Figure 4.2 Binding pocket (P_1) predicted by DoGsite scorer. The amino acids contained in red square represent the active binding site	42
Figure 4.3 Selected binding pocket with multiplicity calculated as 127 generated with RaptorX. The amino acid residues depicted as sticks present in the pocket are labelled.	43
Figure 4.4 The common and uncommon amino acid residues in binding pockets predicted by DoGsite scorer and RaptorX.....	44
Figure 4.5 Visual representation of ligand BC11 docked in uPA binding pocket. Left image depicts the 2D representation of interactions. The right image depicts the 3D representation of ligand protein complex after docking	45
Figure 4.6 Visual representation of ligand BC57 docked in uPA binding pocket. Left image depicts the 2D representation of interactions. The right image depicts the 3D representation of ligand protein complex after docking	46
Figure 4.7 Visual representation of ligand JS62 docked in uPA binding pocket. Left image depicts the 2D representation of interactions. The right image depicts the 3D representation of ligand protein complex after docking.....	46
Figure 4.8 Visual representation of ligand JS67 docked in uPA binding pocket. Left image depicts the 2D representation of interactions. The right image depicts the 3D representation of ligand protein complex after docking	47
Figure 4.9 Visual representation of ligand SR3 docked in uPA binding pocket. Left image depicts the 2D representation of interactions. The right image depicts the 3D representation of ligand protein complex after docking.....	48

Figure 4.10 Visual representation of ligand AB11 docked in uPA binding pocket. Left image depicts the 2D representation of interactions. The right image depicts the 3D representation of ligand protein complex after docking.	48
Figure 4.11 Visual representation of ligand AB5/4 docked in uPA binding pocket. Left image depicts the 2D representation of interactions. The right image depicts the 3D representation of ligand protein complex after docking	49
Figure 4.12 Visual representation of ligand BC11 docked in uPA binding pocket. Left image depicts the 2D representation of interactions. The right image depicts the 3D representation of ligand protein complex after docking	51
Figure 4.13 Visual representation of ligand BC57 docked in uPA binding pocket. Left image depicts the 2D representation of interactions. The right image depicts the 3D representation of ligand protein complex after docking.	52
Figure 4.14 Visual representation of ligand JS62 docked in uPA binding pocket. Left image depicts the 2D representation of interactions. The right image depicts the 3D representation of ligand protein complex after docking.	52
Figure 4.15 Visual representation of ligand JS67 docked in uPA binding pocket. Left image depicts the 2D representation of interactions. The right image depicts the 3D representation of ligand protein complex after docking.....	53
Figure 4.16 Visual representation of ligand SR3 docked in uPA binding pocket. Left image depicts the 2D representation of interactions. The right image depicts the 3D representation of ligand protein complex after docking.....	54
Figure 4.17 Visual representation of ligand AB11 docked in uPA binding pocket. Left image depicts the 2D representation of interactions. The right image depicts the 3D representation of ligand protein complex after docking.	54

Figure 4.18 Visual representation of ligand AB11 docked in uPA binding pocket. Left image depicts the 2D representation of interactions. The right image depicts the 3D representation of ligand protein complex after docking	55
Figure 4.19 Green circle represents results obtained from MOE. Blue circle represents results obtained from GOLD. Orange circle represents results obtained from the previous studies. The three diagrams depict the amino acid residues for three ligands BC11, BC57 and.....	59
Figure 4.20 Statistically significant (19% True positive and 59.3% True negative rate) boronic acid derivative inhibitors pharmacophore model obtained using docking conformations of seven inhibitors aligned with flexible alignment used as a template. The pharmacophore consists of four cationic hydrogen bond acceptors and two cationic hydrogen bond donors with one aromatic ring.	61
Figure 4.21 Selected residues of the binding pocket of uPA with its bound ligand extracted using SPDB viewer. The tube represents the ligand SR3 and the ball and stick model represent the amino acid residues of the binding pocket. For simplicity and clear visualise	64
Figure 4.22 Proposed optimized model complex of uPA binding pocket with ligand SR3. The sticks represent the ligand SR3 while the ball and lines represent the amino acid residues of the binding site.	65
Figure 4.23 The optimized binding pocket of uPA.....	66
Figure 4.24 Optimized geometry of ligand SR3	66

List of Tables

Table 1.1 Many of the pathological effects, arising by shifts in function of uPAR system components, on cancerous cell progression are listed in the specified table [3].	5
Table 2.1 Inhibitors with promising in-vivo metastatic repression in different cancer types.	15
Table 2.2 The calculated interaction energies for the three ligands UI1, UI2 and 172 with urokinase type plasminogen activator are in agreement with the theoretical results that are -107.3 kcal/mol, -99.4 kcal/mol and -35.3 kcal/mol respectively.....	27
Table 4.1 Predicted binding pockets with residues and drug scores generated by DoGsitescorer.	40
Table 4.2 Predicted binding pockets with their multiplicity, top ligands and binding residues generated by RaptorX.....	43
Table 4.3 Structures of the test ligands are given below in the form of ball and stick with the selected conformation from docking results. Binding free energy, electrostatic interaction energy and van der wall interaction energy is given in Kcal/mol	50
Table 4.4 Table representing test compound structures in ball and stick figures along with their generated score through scoring function Gold score	56
Table 4.5 Calculated distance between the features of pharmacophore model.	62
Table 4.6 Computed energies in kcal/mol for optimized geometry, Single point energy and self-consistent reaction field for Sr3 bound uPA binding cavity with the methods used as level of DFT.....	68

Abstract

The plasminogen activator (PA) system is an extracellular proteolytic enzyme system linked with various physiological and pathophysiological processes. A previous literature shows evidence to support that urokinase-type plasminogen activator (uPA) plays a significant role in tumour progression and metastasis. The components of the uPA system show altered expression patterns in several common malignancies, which have identified them as satisfactory diagnostic, prognostic, and therapeutic targets to reduce cancer-associated morbidity and mortality. Proof of uPA inhibition by the seven test ligands have been provided in previous research. However, the binding site and features involved in inhibition of uPA are unknown. Hence it is conducive to design specific inhibitors for the active binding site as an effort to cease the spread further. Fitting computational techniques are used for achieving set objectives. Structure based and ligand based computational techniques and quantum mechanical technique such as Density Functional Theory (DFT) are applied for the characterisation of binding energy and to observe interactions between novel boronic acid derivatives and urokinase-type plasminogen activator. Molecular Operating Environment (MOE) and Gold softwares were used for Molecular Docking simulations and generated results were compared to those of the previous study. The focus was to determine residues of uPA which are involved in high affinity binding to these seven inhibitors. MOE was used for designing pharmacophore model that highlights the descriptors that play important role in high affinity binding of the most promising ligand to receptor protein. Quantum mechanical studies were applied to the test ligand with most favourable binding interactions with the receptor protein, the ligand-protein complex as well as the receptor protein as it is equally important to perform calculations on each structure. Results presented here combine experimental and theoretical works for crafting uPA inhibitors in cancer treatment through a better understanding of the binding interaction of uPA and its inhibitors. Ligand SR3 was chosen as most suitable inhibitor among seven compounds based on docking results obtained through MOE and GOLD with score -3.2481 kcal/mol and 46.4523 kcal/mol respectively. These seven ligands were used for generating pharmacophore model through random selection with genetic algorithm by

MOE having sensitivity of 79% towards the test set, specificity of 78% towards test set and 51% calculated Mathews coefficient correlation. The ready model can be verified for liability through experimental methods. In Computational Quantum mechanical studies hybrid functional B3LYP in conjunction with basis set LANL2DZ of Density Functional Theory (DFT) on the extracted model of uPA binding site with ligand SR3 were applied based upon the electron density of uPA to find the binding energy of active ligand. A -2 charge is present on ASP189 of the binding cavity throughout the DFT simulations. From the computational analysis Geometric optimization (opt) gave values of 53.9 and single point energy (SPE) as -66.3 with self-consistent reaction field (SCRF) with calculated value of -49.0. Hence it is concluded that SR3 shows better binding with uPA binding pocket and there is a negative two charge on it ASP189 amino acid residue in the binding pocket.

1 Introduction

1.1 Cancer

Cancer is a broad expression disease that is caused due to cellular modifications resulting in abnormal growth and cell proliferation. About 14 million people around the globe are diagnosed with cancer. Cancer has a mortality rate of millions per year and remain the most fatal of killers among all diseases [1]. Many efforts are being put in coming up with advanced and innovative diagnostic tests and treatment options [2]. Cancer metastasis is the start of last stages of tumorigenesis; it is the dissemination of diseased cells from the site of origin through detachment, followed by the movement towards other sites for invasion by blood vessels or lymphatic vessels. In these far-flung sites, these diseased cells settle for further growth and spread [3]. To understand metastasis, it is essential to understand the events occurring behind it at the molecular level, which will eventually lead to effective treatment of cancer at later stages.

Although the survival rate of cancer patients has improved considerably owing to a great deal of research and work being done in this field for early diagnosis. Nonetheless, the morbidity rate is still high, especially if the cancer has metastasised, stage 4 cancer is responsible for about 90% of cancer deaths.

Cancer metastasis is an outcome of a cascade of interdependent stages taking place in the tumour micro-environment as described in Figure1.1 which comprise of the following steps:

- The detachment of primary tumour cells from the original site.
- Circulation through lymphatic/blood vessels to distant organs.
- Cancer cells, after reaching the distant organ adhere to basement membrane or capillary endothelial cells, invading the surrounding tissues, which would consequently lead to the degradation of extracellular matrix (ECM).
- These steps are followed by extravasation of the diseased cell to gain access to lymphatic/blood vessels.
- Proliferation within the distant organ is the last step to metastatic invasion [4].

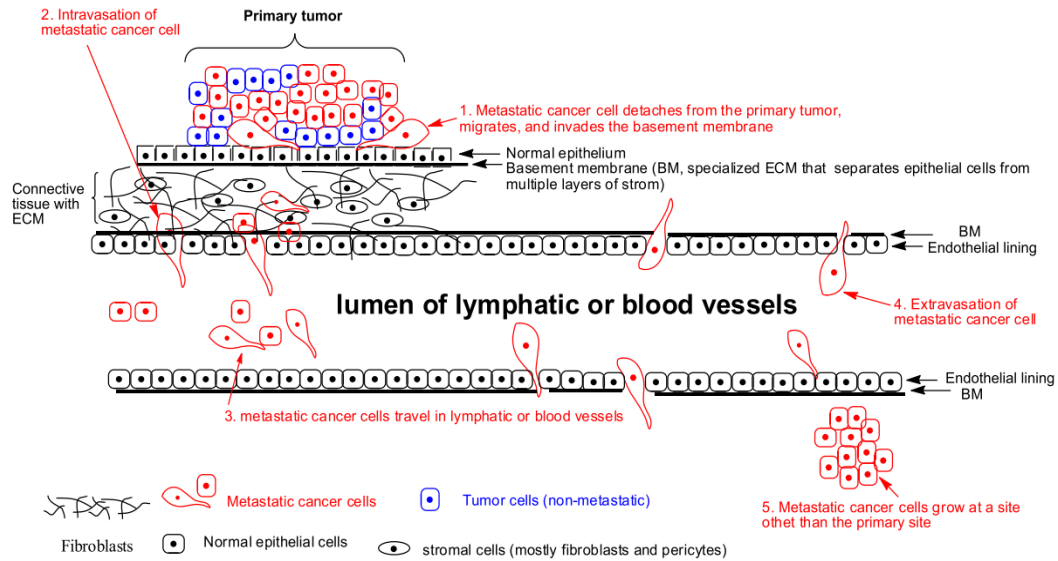


Figure 1.1 Presentation of steps involved in a metastatic cascade [3]

The role of the tumour microenvironment (cancer-associated fibroblasts (CAFs), immune and inflammatory cell, genes involved in blood and lymphatic vascular networks, extracellular matrix structure and growth factors) and its involvement in cancer progression and invasion is well understood. Hence, tumour microenvironment and the components involved in metastatic processes are considered as potential targets for the prevention and inhibition of metastasis[5].

The active components of urokinase-type plasminogen activator (uPA) indicated to take part in cancer progression are being targeted for development and preparation of potential drugs from inhibitors providing promising outcomes through wet-lab experiments and reviewing computational results of binding interactions with the receptor along with its pharmacokinetic properties. These proteins belong to the vast family of proteins labelled as serine proteases.

1.2 Serine proteases

Serine proteases cover the most substantial portion of known proteolytic enzymes present in nature, having 800 deposited structures in Protein Data Bank (PDB) out of which one third being thrombin and trypsin [6]. These functionally diverse enzymes are present in every cellular life form, including numerous viral genomes [7]. The widespread family of

proteolytic enzymes receive considerable attention from researches because of their crucial role in the control of a variety of biological processes such as DNA replication and transcription, wound healing, blood coagulation, stem cell mobilisation, cell proliferation, tissue remodelling, neurogenesis and apoptosis. Any type of shift in the proteolytic processes may lead to adverse pathological disorders including inflammatory and cardiovascular diseases, neurodegenerative disorders and cancer [8]. One of the systems showcasing its role is the urokinase-type plasminogen activation receptor (uPAR) system.

1.3 Urokinase-type plasminogen activator receptor system (uPAR)

The plasminogen activator (PA) system is an extracellular proteolytic enzyme system associated with various physiological and pathophysiological processes. A large body of evidence support that among the various components of the PA system, urokinase-type plasminogen activator (uPA), its receptor (uPAR), and plasminogen activator inhibitor-1 and -2 (PAI-1 and PAI-2) play a major role in tumour progression and metastasis [4], [9]–[12].

The binding of uPA with uPAR is instrumental for the activation of plasminogen to plasmin, which in turn initiates a proteolytic cascade to degrade the components of the extracellular matrix (ECM), and thereby, cause tumour cell migration from the primary site of origin to a distant secondary organ [13]. The inactive pro-uPA circulating in plasma and extravascular fluids binds to glycoposphatidylinositol (GPI) anchored urokinase receptor (uPAR) attached to the cell membrane, hence converting the zymogen plasminogen to active plasmin which would successively activate the pro-matrix metalloproteases (MMP). Plasmin and active MMPs stimulate the breakdown of the ECM PAI-1, PAI-2 are endogenous inhibitors against plasminogen [9]. The urokinase-type plasminogen activation system is known to have a hand in various processes of cancer such as angiogenesis, cell invasion and metastasis, inflammation etc. [14]. Figure 1.2 in the following text describes the activation of zymogen pro-uPA into uPA as it binds to its endogenous GPI anchored receptor uPAR. Activated uPA allows the activation of plasmin from its inactive state plasminogen that is involved in the degradation of ECM and activation of the MMPs.

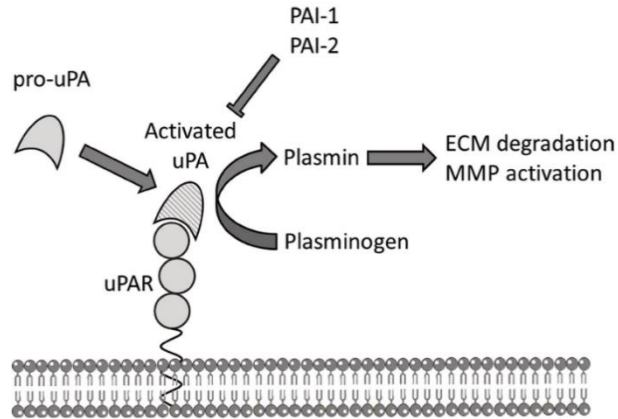


Figure 1.2 Urokinase-type plasminogen activation system in action

Plasminogen plasmin system is known to have a vital role in the diseased cell progression known as metastasis during cancer along with poor prognosis, that makes it conducive to design specific inhibitors for the active binding site as an effort to cease the spread further. Table 1.1 provides the data showcasing the biological effects expressed by each component of the uPAR system according to different cancer model systems in which they are linked.

Introduction

Table 1.1 Many of the pathological effects, arising by shifts in the function of uPAR system components, on cancerous cell progression are listed in the specified table [3].

Cancer type	Components of uPAR	Observed biological effects
Oesophageal	uPA	Increased metastasis
Oral	PAI-1	Promotion of initial stages of oncogenesis
Gastric	uPA, uPAR	Poor prognosis, increased angiogenesis
Colorectal	PAI-1, uPAR	Poor prognosis, increased motility
Rectal	uPAR	Poor prognosis
Pancreatic	uPA, uPAR	Poor survival, Tumour growth and metastasis, rapid progression
Small cell lung	uPAR	Improved survival
Mesothelioma	uPAR	Tumour promotion
Osteosarcoma	uPA, uPAR	Tumour growth and metastasis
Chondrosarcoma	uPA, tPA, PAI-1	Aggressive cancer, Metastasis
Melanoma	PAI-2	Inhibition of apoptosis
Breast	uPA, PAI-1	Poor survival, metastasis and advanced tumour, poor prognosis
Endometrial	uPAR	Aggressive cancer
Cervical	uPA	Poor prognosis
Ovarian	uPA	Metastasis
Prostate	PAI-1, uPA, uPAR	Inhibition of tumour, angiogenesis, and metastasis
Renal	uPA, uPAR, PAI-1	Tumour progression
Glioma	uPA, uPAR	Poor survival, Tumour growth and angiogenesis
Pheochromocytoma	uPAR	Mitogenic
Leukaemia	uPAR	Increased invasiveness, aggressive cancer

1.4 Boronic Acid

Boron is an abundant and low toxic compound which facilitates its use in a variety of fields such as organic chemistry, biological sciences, material sciences and medicine. Boron is a metalloid present next to carbon on the periodic table has a symbol **B** and an atomic number **5**. The electronic structure of boron allows it to exhibit diverse chemical features presenting some similarity and differences with that of carbon. These characteristic traits make it important in medicinal applications [15].

Boron has been considered as one of the most valuable elements in the nature since the mid of 19th century, mainly due to its vacant p orbital due to which it can have a reversible covalent interaction with heteroatoms like oxygen and nitrogen. Due to this chemical property, it is being used as a target for nucleophilic residues in diseased proteins, thus allowing it to be a remarkable medium for manufacturing value-added products. Regardless of accessibility, natural products lack the carbon-boron (C-B) bonds. One might think of its uselessness due to this feature; however, its low toxicity marks it treasured in synthetic chemistry and drug discovery. This attribute makes boron a potential candidate in drug discovery [16].

Boronic acids are derived by the sequential hydrolysis of a borane as portrayed in Figure 1.3 [17]. The first step is the conversion of borane to borinic acid, which has one of the three carbon groups replaced by a hydroxide group. Borinic acid being more stable than the precursor is liable to the second hydrolysis that leads to the formation of boronic acid, which is a boron centred chemical structure having two hydroxyls and one R group, respectively. It is being used in various synthetic reactions such as Suzuki–Miyaura coupling (C–C bonds) and hydroboration (C–H, C–OH bonds) and several drug discovery studies i.e. in medicinal chemistry [18].

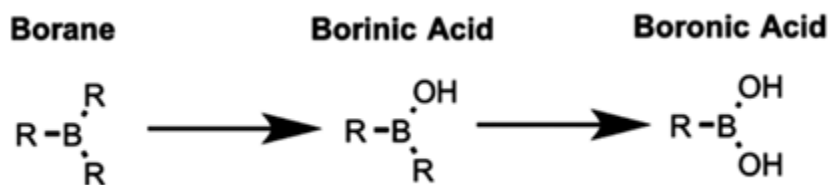


Figure 1.3 Borinic and boronic acids are organoboron species derived from borane [17].

Boronic acids might also be derived through other methods, some of them being metal-halogen exchange reactions, trans-metalation and coupling of di-boronyl species with aryl halides. The boronic acids show higher stability than both the predecessors which on oxidation would give boric acid as a resultant that is used in many household items such as glue, eye drops, saline solution, liquid starch, insecticides and many laundry detergents. When boronic acids are in their neutral state, they have a central boron displaying trigonal planar sp^2 hybridized geometry with an alkyl or aryl group and two hydroxyl groups attached, resulting in six valence electrons around boron, an exception to the octet rule [19].

1.4.1 Derivatives of Boronic acid as protease inhibitors

Boronic acids do not exist in nature; rather these abiotic compounds are a result of two-fold oxidation of their natural occurring precursors like boric acid, synthetically [22]. Boronic acids have valence electrons that can form off-target toxicity as they would react with endogenous nucleophiles; therefore the outcomes are in the form of below standard pharmacokinetics. Many studies from the literature suggest boron-based warheads with stabilised functionality along with reduced toxicity for example in the form of aromatic boron-based heterocycles, their ester derivatives, 6- Substituted hexamethylene amiloride (HMA) derivatives and their multipurpose conjugates which are beneficent therapeutically [23][24][25]. The carbon group directly attached to the boron atom determines its properties and chemical reactivity (Figure 1.3).

For the benefit of understanding, we classify the boronic acids according to their respective functional groups such as

- Alkyl-boronic acids,

- Alkenyl-boronic acids,
- Alkynyl-boronic acids,
- Aryl-boronic acids [22].

Bortezomib and Ixazomib are Boronic-acid based proteasome inhibitor, Food and Drug Administration (FDA) approved drugs, which are being used for fighting cancer [20]. They can be considered as a template for understanding the pharmacokinetics and role of Boronic-acid ligands in the process.

1.5 Computational techniques applied

In today's modern world of powerful tools, the structure-activity relationship (SAR) of potential drug-like compounds is being studied using advance chemistry methods together with molecular modelling [21]. Researchers search into pharmacodynamics as well as pharmacokinetics of a drug like compounds while putting the computational techniques to use [22]. During potential drug development, it is of benefit to have vital structural information about the drug target. Over 100,000 three-dimensional protein structures, nucleic acids, and complex assemblies are available owing it to bio-molecular spectroscopy techniques. There is an excellent advancement in structural and molecular biology as a result of progression in these techniques such as nuclear magnetic resonance (NMR) and X-ray crystallography providing resolution of many protein structures [23]. Powerful and highly developed computational tools in the field of drug design have been designed for sorting, managing, and examining the accessible data. In the light of provided information, fitting *silico* and experimental techniques are incorporated for better understanding of the complex characteristics of intermolecular recognition [24]. To achieve the mentioned goals, two beneficial practical approaches in drug discovery are

- Structure-based drug design (SBDD) [25]
- Ligand-based drug design (LBDD) [26]

In modern pharmaceutical chemistry, structure-based drug design (SBDD) is the primary approach which employs available information on existing three-dimensional structures of the target in crafting novel drug-like compounds. Some widely applied strategies are

structure-based virtual screening (SBVS), molecular docking and molecular dynamics (MD). These techniques are operated in a broad range of applications such as calculation of binding free energy, binding conformational changes and noncovalent molecular interactions. On the other hand, ligand-based drug design (LBDD) techniques use libraries that comprise a unique and diverse biochemical data of small-molecules that are well-known for binding with their specific targets in virtual screening, sequence similarity searching, pharmacophore models and quantitative structure-activity relation (QSAR) [25].

The mentioned techniques, however, lack studying the electron-based properties for which quantum mechanical (QM) methods such as density functional theory(DFT) are developed that efficiently describes the drug-receptor microenvironment at a realistic cost.

Molecular docking simulation, pharmacophore modeling and density functional theory calculations are being applied to infer the binding interactions between the ligands and target protein based on residues involved in binding along with their binding energies.

1.5.1 Structure based drug design (SBDD)

1.5.1.1 Docking

Molecular docking approach is used in modern drug design for approximating binding free energy of a ligand-protein complex along with conformational poses generated by a ligand within the binding pocket of a target protein. Diverse computer programs and algorithms are available for performing molecular docking. However, one must be familiar with the advantages and disadvantages of each algorithm which would pave the way in the progression of efficient procedure that would ultimately lead to relevant results [25].

1.5.2 Ligand based drug design (LBDD)

1.5.2.1 Pharmacophore modelling

Ehrlich in the 19th century first defined the term “pharmacophore” as “a molecular framework that carries the essential features responsible for a drug’s biological activity”. From here, it can be concluded that a pharmacophore model points towards the essential features a potential drug like compound primarily possess. The model would be a depiction

of the significant features such as electron acceptors and donors, the position of the compound in a binding cavity along with its direction [27]. After that, Schueler, laid the foundation for modern pharmacophore; its beginning and our apprehension. The International Union of Pure and Applied Chemistry (IUPAC) later defined pharmacophore as, “*the ensemble of steric and electronic features that is necessary to ensure the optimal supramolecular interactions with a specific biological target structure and to trigger (or to block) its biological response*”. Commercial, as well as free computer programs are available for building a pharmacophoric pattern based on the 3D alignment of ligands. Some examples of such programs are MOE, LigandScout, Corina and medchemstudio [28].

1.5.3 Quantum mechanical methods (QM)

1.5.3.1 Ab initio QM

Ab initio quantum mechanics being implemented since the past three decades has become an unavoidable technique in quantum chemistry while working on complex polyatomic and molecular systems especially in fields such as biology and materials science and engineering. Everything revolves around finding an appropriate solution for the Schrödinger equation if information such as the total number of electrons along with an assortment of points where the atomic nuclei are lying in a molecular system, its electron density and energy along with additional properties being defined with the help of “model chemistry” that are precise, unambiguous mechanical approximations. In 1998, John Pople and Walter Kohn were awarded the Nobel prize for their portion of work on the *ab initio* molecular orbital theory and density functional theories that were based on the concept laid by Schrödinger and Paul Dirac in the year 1926 who were awarded the Nobel prize in 1933. The solution for Schrödinger equation for a system with more than hundred atoms modernised the theoretical chemistry in finding solutions with great accuracy by applying refined codes and effectual algorithms in varied disciplines [29]. Using computational *ab initio* techniques for large proteins regarded in aqueous solutions is expensive due to which its application is limited. Therefore, as alternative small selected parts of the whole system are treated by the *ab initio* quantum mechanics. In contrast, the rest of the system can be analysed relatively by molecular mechanics (MM) methods or implicit solvation methods.

The integration of the quantum mechanical methods with the additional models obtained from the MM and the self-consistent reaction fields (SCRF) methodologies have become an illustrious element of the theoretical armament which allows the user to construct accurate models of the large intricate molecular structures [30].

1.5.3.2 Density Functional Theory

In the present day, a lot of tools and methods have been realised making computer-aided drug design better than before. One of those methods is density functional theory (DFT) that is agreeably crucial for the drug design development. Ab-initio DFT approach has established an innovative "computational microscope" that gives a detailed insight to the biologically pertinent molecules and compounds thus providing a model closest to the novel structure [31] at an affordable computational cost relative to the other techniques which makes it a vastly applied method in computer-aided drug designing [30], [32], [33]. This technique is regularly exploited in a wide variety of fields that are far-off from the quantum mechanics such as mineralogy, classical fluids, superconductivity, electronic band structures in solid-state physics, magnetic properties of alloys and to our concern the binding energy of molecules in computational chemistry are being calculated by using DFT processes [34]. While molecular mechanics (MM) methods have been magnificently employed conventionally throughout computer-aided drug design and development but still these techniques have been failing at some points when applied to understand the electron arrangement and its properties in the molecular microenvironment of the drug-receptor binding. This dilemma has a solution by choosing the quantum mechanical techniques. However, these computations are often too exhaustive, which makes it an unsatisfactory choice for medicinal chemists. Nevertheless, in the past five years, this quantum mechanical method has been applied to pharmaceutical complications which have proved to be a diligent and efficient method. Molecular mechanics treat atoms as charged expandable balls connected with a spring and essentially deals with the nuclei while in quantum mechanics the properties of electrons are the centre of attention. In QM the wave function (Ψ) holds the complete information about a system under investigation. The Schrödinger equation ($H \Psi = E \Psi$, where Ψ is the wave function) is the highlight of the QM. If the wave function for a system is identified or known, then it is possible to find out

the physical properties of the structures under study. The molecular orbital quantum mechanics simulations deliver rough solution for large drug like molecules wave function. The wave function (Ψ) for a drug like polyatomic molecular system is the product for one-electron wave functions (ϕ_i). ϕ is the three-dimensional empirical function that is used for the properties and energy of each individual electron in a drug like molecule. The unidentified molecular orbitals of the drug molecule can be denoted by generating the linear combination with the help of the already known atomic orbital functions (χ_i) [33].

1.5.3.3 Semi-empirical methods

Semi-empirical quantum mechanical methods are the computations of much larger systems that cannot be computed by using the *ab initio* approaches or the DFT, another method mentioned above, i.e. the molecular dynamics simulations are also appropriate for more extensive system if the computational expense is in accordance with the correctness. However, even if they can be applied to the larger molecular bodies, they do come with a limitation being less truthful exclusive of the situation where the procedure is being applied to a specific property with the associated parameters being assigned [30]. Being conscious of the situation where Schrödinger equation is unsolvable for systems with many atoms hence there came a need of designing semi-empirical *ab initio* DFT techniques for the estimation of the quantum mechanical resolutions to the complication. Although, the QM simulations are the rigorous models but are the most expensive and time consuming ones as well, hence being put in practice for minute systems with not many atoms [35].

1.6 Problem statement

Since Plasminogen Plasmin system has a key role in spreading cancerous cells to other parts and organs of the body during cancer and contribute to poor prognosis that makes it conducive to design specific inhibitors for the active binding site as an effort to cease the spread further.

1.7 Objectives

The direct aims of this dissertation are to achieve the objectives listed below:

- Analyse the ligand-protein interactions of the urokinase type plasminogen activator (uPA) with its seven test ligands through computational technique, molecular docking, which would further provide an insight into the properties of the considered ligands.
- To discover the crucial features significant in binding hypothesis by generating a pharmacophore model through computer aided drug design (CADD) to promote the search for active compounds in the compound library.
- A Quantum Mechanical (QM) method known as Density Functional Theory (DFT) method is utilised as it gives accurate results. Also, it is cost efficient as compared to other costly techniques and consumes relatively less time for structure elucidation and studying the binding interaction between the seven test ligands and the binding pocket of the protein of interest. However, there exist some limitations, like all the other known techniques to drug design methods.

2 Literature Review

The focus of this thesis is to investigate the binding interactions between seven novel boronic acid derivatives and its bio esters with target receptor uPA. The previous results obtained from in silico and in vitro studies are of utmost importance and acknowledged. Drug discovery and development is an exhausting and tedious task where drug demands are high, and the process is a hit-and-trial course. However, computational chemistry has made it that much acceptable and realisable by utilising sophisticated drug discovery tools proving to be a great help in medicinal chemistry as well as academic research purposes. Nevertheless, pursuit for selecting potential drug candidates i.e. initial hit compounds and analysing their multifaceted protein-ligand interactions requires high efficiency and precision which makes the classical empirical methods inadequate[35]. The deep-rooted attentiveness towards efforts to suppress tumour progression has led to designing novel uPA inhibitors. As an upshot of the hard work put in this field, various compounds and their derivatives indicated positive results such as antibodies or peptidomimetics depicting inhibition of metastasis and tumour growth in mice models as presented in Table 2.1 [36]–[38] These achievements motivated researchers in hope of finding least toxic and efficient compounds capable of drug like properties. The plasminogen activator (PA) system together with its components is one of the strongest diagnostic and prognostic factors having level-of-evidence-1 in breast carcinoma [39].

Table 2.1 Inhibitors with promising in-vivo metastatic repression in different cancer types.

Related Cancer	Treatment/ Inhibitors	Outcome	Reference
Breast cancer	Amidino phenylalanine-type uPA inhibitor (WX-UK1)	Suppresses metastasis in rat breast cancer with reduced primary tumour growth	[37]
Lung cancer	Amidine-based, peptide-derived inhibitor	Suppresses metastasis in fibrosarcoma model in mice	[40]
Transgenic mammary cancer	Hybridised uPA-deficient mice	Suppresses metastasis	[41]
Colon cancer	Antisense inhibition of uPAR	Suppresses invasiveness	[42]
Human melanoma, prostate cancer	Antisense oligonucleotides for uPAR	Inhibition of metastasis in human melanoma and bone metastasis in mice	[43]

2.1 Role of uPA and uPAR in cancer

There have been various studies on trying to understand the logic and mechanism of tumour cell progression, along with hard work done in the field of pharmaceuticals trying to develop fewer toxic inhibitors for halting pathogenic cell invasion and growth. Researchers are now confident about the direct relation of uPA levels with the tumour cell migration and invasion [12], [13], [44]–[46] while the overexpression of uPA system components is directly linked to poor survival and recovery rates [47]. The literary texts presented by several researchers are in alignment with the hypothesis mentioned above, therefore draws quite a lot of attention towards the uPA system [48]. uPA does not possess a transmembrane domain due to which it is dependent upon its indigenous receptor and other components such as vitronectin, for cell signalling and Extra cellular matrix (ECM) degradation. Such interactions are accounted for enabling the role of uPA in tumour

progression and angiogenesis by different studies in the literature. Due to the linkage of uPA-uPAR, there is an accumulation of the cell surface receptor uPAR promoting interaction with vitronectin which further exacerbate ECM degradation along with promotion of tumour cell migration to distal organs, angiogenesis and invasion [49].

Cells in living organisms are held together by a three dimensional network known as extracellular matrix (ECM) composed of proteins, glycoprotein and enzymes which provide systematic sustenance to the cells and regulates cell performance by determining cell movement, propagation, and differentiation [50]. During normal processes such as regeneration of lacerations, organ homeostasis and wound healing the ECM undergoes remodelling process which includes degradation and assembly. If any of these courses become abnormal, they play a major role in lethal diseased conditions.

An example is the stiffening of the stromal cell in tumors [51]. Kandice *et al.* stated in 2009 that ECM in breast cancer tissue is sturdier with high collagen cross-linking [52]. For the remodelling of ECM, two coherent approaches are: either by elimination of a component protein that is involved in building up the 3D matrix of ECM, or by tempering with the structure or assemblage of the ECM system by reorienting enzymes that are directly involved in the structuring. Proteinases present in the extracellular environment playing a key role in revamping or degradation of ECM are listed as follows:

- Serine proteases e.g. plasmin and cathepsin G
- Matrix metalloproteinases (MMPs) have four subgroups: collagenases, stromelysins, gelatinases and membrane type MMPs
- Disintegrin and metalloproteinase with thrombospondin motifs (ADAMTS)
- Metzincin proteinases

The subgroups of MMPs altogether are proficient in complete breaking down ECM and basement membrane (BM). Among the protein degrading enzymes, a type of serine proteinase known as plasmin is responsible for the activation of growth factors and MMPs. These events assist in tumor cell metastasis and invasion, an increase in the plasmin levels during these processes is observed which is an outcome of overexpression of the urokinase-

type plasminogen activator. Inferring from the recorded results and literary work, it seems that selecting these enzymes as target for designing a therapeutic approach in an attempt to prevent cancerous cell growth and mobility is an effective perception [53].

Cantero *et al.* (1997) investigated high level of expression of uPA and uPAR in pancreatic cancer in humans. Several test techniques were applied to evaluate over expression of uPA and uPAR in diseased cells and the results achieved strengthened the theory. It was observed that 70% of the selected specimen from pancreatic cancer exhibit six times elevated expression of uPA mRNA and four times elevated expression of uPAR mRNA through Northern blotting technique. The diseased cells also disclosed concurrent existence of uPA and uPAR through Immunohistochemistry (IHC) study. The spots harbouring invasive tumorigenic cell in some pancreatic ductal adenocarcinoma, such as the stromal and ductal cells and the acinar cell going under atrophy showed high immunoreactivity towards the labelled antibodies used in immunostaining. uPA and uPAR in surroundings with malignant abrasions were also prone to immunoreactivity. The test results were accord to the previous publications claiming the influence of uPA system components (i.e. uPA and uPAR) on poor patient prognosis along with their elevated co-occurrence at the protein level [54].

2.2 Inhibitors developed against uPA

Search for compounds that might halt the activity of uPA and possibly its interaction with its endogenous receptor (uPAR) began as soon as its involvement in angiogenesis and metastasis was elucidated. Numerous research articles are published discussing diverse groups of inhibitors designed against uPA but then again lacking in one way or another.

Initially, peptide aldehydes were the compounds used as inhibitors to deteriorate the action of cellular proteases which showed successful inhibition but were considered ineffective due to their off-target binding with proteasomes causing toxicity later on. Apart from drug toxicity, it failed in bio-availability and stability [55]. However, in 2010 Julian Adams *et al.* reported another significant progress when the derivatives of these compounds (peptide boronates) were developed which proved to have improved potency against uPA [56]. The

Literature Review

empty p-orbital on boron is accredited for the improved potency by accepting a lone pair of oxygen present on the serine residue of the binding pocket [57]. As the pico-molar range of the potencies was observed to be short, this provided the opportunity to truncate the inhibitor molecule without losing the potency and maintain an effective inhibition quality like in case of dipeptidyl boronic acids having a phenylalanine at P2 position. As compared to the concise peptide boronates, the dipeptidyl aldehyde compounds require a bulky chunk of hydrophobic P2 residues (naphthyl alanine) for an efficient inhibition with great potency.

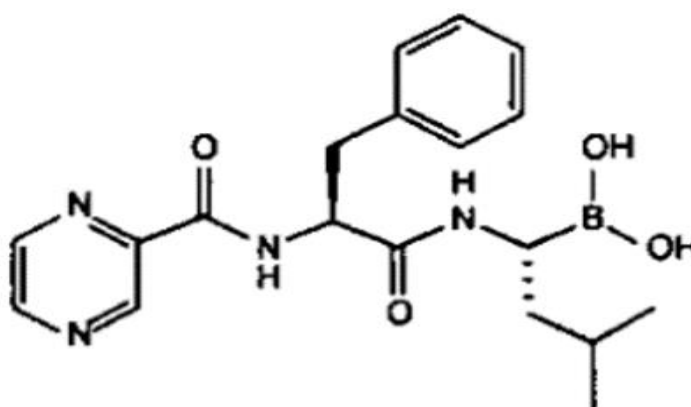


Figure 2.1 Compound 15 [57]

When analysing the compound number 15 (dipeptidyl boronic acid) given in Figure 2.1, the low molecular weight provides benefit over the bulky compounds that cannot fit in the slim binding cavity of serine proteases and has a rationalised synthesis. The key fact that gives these compounds such a reputation is their high selectivity towards serine proteases is that the inhibitor to show interactions with residues present in the S3 and S4 binding subsites in enzymes such as elastase and chymotrypsin for producing maximum inhibitory activity which cannot be observed in the dipeptide inhibitors. Conversely, thrombin has a liking towards the basic residues that are residing within the P1 region of the catalytic region. Hence, does not show break in activity with inhibitors having leucine boronic-acid at the mentioned position [57].

In 2017, Xue *at el.* and his colleagues presented their work showcasing the inhibition of uPA by a member of flavonoid known as Quercetin with IC₅₀ value of 7μM [58]. They

presented the molecular function mechanism for the inhibition of uPA with flavonoid inhibitors for the first time. Crystal structure using X-ray crystallographic technique was used during the study to mould Quercetin:uPA complex in which recombinant protease domain exhibiting activity like the two chain uPA was used.

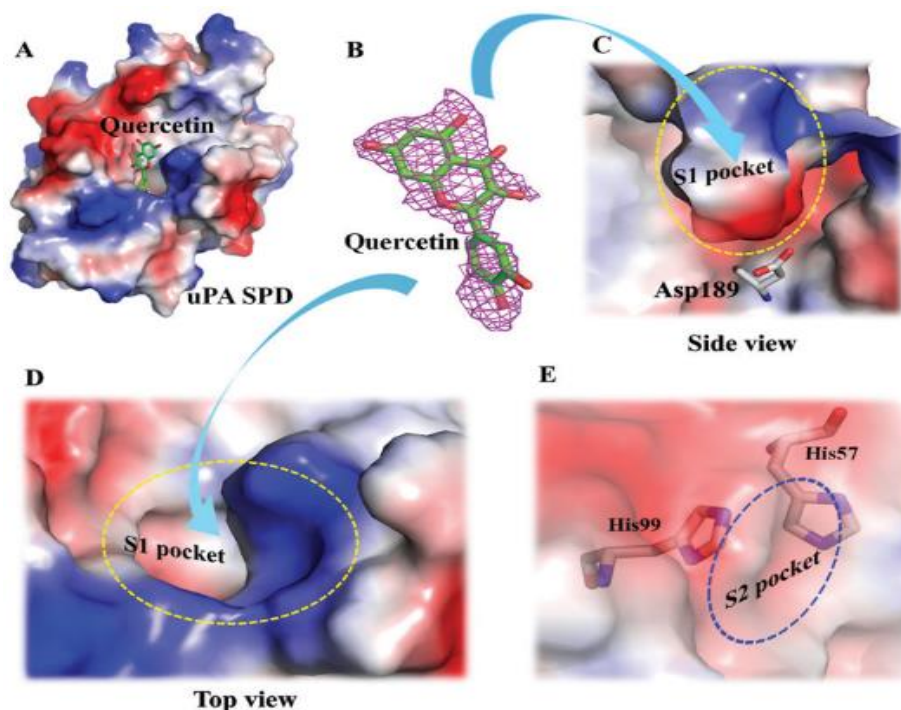


Figure 2.2 A. Quercetin bound to the binding pocket of uPA. B. Electron density map around Quercetin molecule as magenta web. C. Asp189 residue depicted in stick form at the bottom of S1 binding site shown from side view with electrostatic potential surface. D. Top view of the binding pocket. E. Interacting amino acids in the S2 pocket [58].

It was evident from their results that quercetin did yield interaction in the binding pocket of uPA which can be observed in Figure 2.2 given below. 71.4% of quercetin surface area is involved in the binding which can be observed by the electron density map as shown in Figure 2.2B. Figure 2.2C and 2.2D depicts the attachment of B ring of Quercetin in the S1 binding site while the base of S1 site is occupied by two adjacent phenolic hydroxyl groups (catechol) at positions B3' and B4' forming hydrogen bonds with the residues Aspartate(ASP)189, Serine(SER)190 and Glycine(GLY)219. The S2 site is occupied by the two hydroxyl groups that are present on the A ring of quercetin as depicted in figure 2.2A and 2.2E. Other interactions such as hydrophobic interactions of aromatic ring with

Literature Review

Tryptophan (TRP)215 and Glutamine (GLN)192 residues of uPA as shown in Figure 2.2B are essential for facilitating the ligand receptor binding. Three oxygen atoms of quercetin located at position A and C rings are responsible for forming dipole-dipole interactions with Histamine (HIS)57 of the catalytic triad HIS57, ASP102 and SER195 as depicted in the figure 9A. It was suggested that, inhibition of uPA might be due to the direct interaction of quercetin with HIS57 that acts as a catalyst by eliminating a Ser195 proton [58].

Along with the progression of finding novel inhibitors, boronic acids started to gain importance in drug design and can be witnessed in a number of drugs approved by FDA e.g. Bortezomib and Ixazomib [20]. Pharmacists want to bring to light the efficient boronic acid inhibitors that form reversible covalent interactions with the target protein [56]. Bortezomib was the first specific proteasome inhibitor in 2003 that was advanced to phase II clinical trials for a number of cancerous tumours along with haematological malignancies such as chronic lymphatic leukaemia, prostate cancer, pancreatic cancer and colon cancer [55]. It was reported to show quick elimination from the vascular compartment; however a pharmacodynamics assay revealed the capability of bortezomib to bind reversibly with the target (proteasome) which has dose dependent inhibition and controllable toxicity. Adams *et al.* gave evidence in 2004 supporting their results. On the basis of these physicochemical properties of bortezomib, an immunochemical assay is developed and utilised for providing accurate and sufficient dose of the compound in phase I studies and deduce the proteasome activity from blood or only white blood cells along with the antagonist drug potency values. The assay is an analytical instrument for keeping the dose escalation in supervision. The immunochemical assay testing in subjects suggested low discrepancy between inter-subject and intra-subject proteasome activity. They concluded that the activity of the drug was evidently dependent upon the dosage of the drug and a dosage of 1.96mg/m² resulted with 80% proteasome inhibition. Rat models were used for further investigation, the drug was given to rats which showed even distribution of the drug in most of the organs by whole-body autoradiography and immunoassay testing. However, the drug was not detected in the eyes, testes, or the central nervous system of the animal models. During further analysis with bortezomib in other animal model such as rodents and primates, it was observed that the activity of proteases was

restored after 48 to 72 hours once the treatment was discontinued [55]. Keeping the previous achievements in mind, it can be suggested that boronic acid and their derivative might prove useful in designing novel drugs.

2.3 Cutting-edge techniques used for finding effective inhibitors for uPA

Bioinformatics is comparatively a new field that is co-evolving with the two subjects: biology and computer science. Mathematical and computer science methods are being carefully put to sense to crack problems in molecular biology that involves large scale data sets, computations based on mathematical algorithms, and analysis research area [59]. There are two types of approaches in discovering and developing chemical compounds into drugs.

- Structure based
- Ligand based

Different *in silico* methods for investigation of the interactions between ligand protein complex established on the structure and ligand-based approaches can be observed from different studies, some of which are mentioned below.

2.3.1 Structure Based studies for uPA

Emil Fischer proposed the hypothesis of “lock and key” which laid the foundation of structure-based drug design 100 years ago . Many inhibitors have been designed in the past by applying the information derived from structure/activity analysis. A three-dimensional structure that might be obtained by NMR spectroscopy or X-ray crystallography of the target protein is required in structure based studies for retrieval of the information in discovering and developing novel inhibitors [60]. However, if the three-dimensional structure is not available, we can always opt for homology modelling in the *de novo* design.

2.3.1.1 Structure of Urokinase type plasminogen activator (uPA)

uPA belongs to a broad family of proteins known as serine protease. It is involved in tissue remodelling processes in multiple normal and pathological conditions [61]. For executing the said processes it is necessary that matrix metalloproteinases (MMP) be activated which would now vitiate the basement membranes and the components of the extracellular matrix. The zymogen pro-uPA is cleaved at the point where lysine(LYS)178-Isoleucine(ILE)179 bond (Uniport/Swiss-Prot entry P00749) is present after binding to its specific cell surface receptor uPAR. This is how it is converted into a two-chained active form of uPA that would eventually activate the plasminogen to broad range plasmin for proteolytic activities [62], [63].

There is modularity in design of the uPA, that is in its activated form, which is composed of three domains being

- Growth factor like domain
- Kringle domain
- Catalytic domain

The pathway presented in Figure 2.3 mainly provides a docking region for its chief substrate plasminogen having very high substrate specificity.

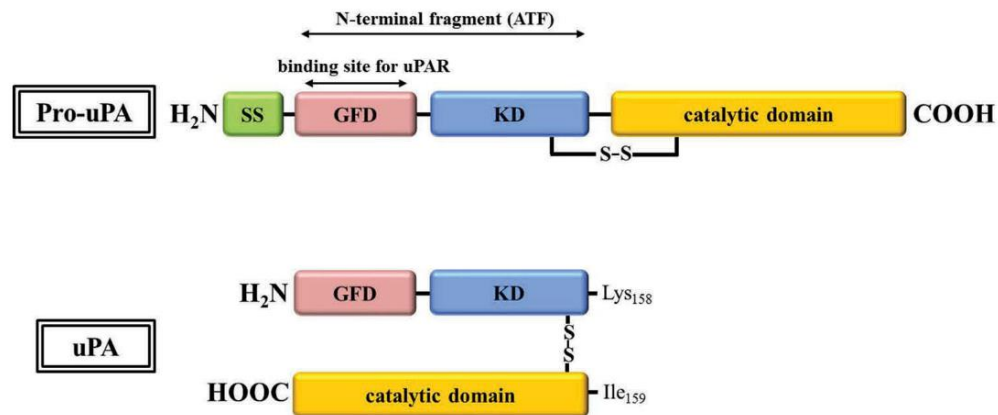


Figure 2.3 Representation of the three domains of pro-uPA and uPA. Pro-uPA is a single chain precursor that is cleaved at peptide bond between Leucine158-Isoleucine159. Active form of uPA has two-chains.

Gene coding for uPA is (PLUA), which during expression process is meticulously controlled by different mechanisms such as post-transcriptional mechanism and epigenetic mechanisms such as DNA methylation, modification of the histones plus regulation of the noncoding ribonucleic acid. There are two regions governing the PLUA transcription respectively: the proximal minimal promoter region rich in GC/GA content which is upstream of the TATA box and recognised by omnipresent transcription factors, the second factor being the upstream enhancer element [49].

More than a few elements are recognised in the 5' flanking region of the transcribed region as regulatory factors serving the regulation of uPA expression. These mechanisms provide elevated chances of the disease cell progression due to the tenacious overexpression of uPA in a diseased condition. Keeping in mind the previous facts it has been suggested that uPA play an important role in cancer invasion and metastasis [54].

2.3.1.2 Molecular docking studies for uPA

In 2014 Sulimov *et al.* worked on exploring and developing new uPA inhibitors as antitumor drugs through molecular modelling in computer aided structure-based drug design [64]. The small drug like compounds can bind to the receptor protein efficiently and inhibit their biological activity. Through docking with SOL program, the ligand-receptor binding free energy can be predicted that is associated to the inhibitory effect of the ligand. Ligand poses are searched within the binding cavity of receptor protein through global optimization of ligand-receptor potential energy in docking. The calculations are expected to be less time consuming in SOL if:

- There is no degree of freedom in the receptor protein with broadened atomic potential with range of 0.3- 0.4 Å to be conscious of partial flexibility of atoms.
- Docking cube is used to cover all the active site atoms.
- Born model is used for de-solvation energy calculation through grid potentials.
- SOLGRID program has an already calculated uniform space grid for the potentials of the receptor atoms that is utilised in calculating the ligand-receptor binding energy.

- When searching for ligand binding poses local energy optimization is excluded.
- When searching for ligand binding poses bond angles and lengths are fixed.
- The scoring function is a weighted sum of the entropy components and ligand-receptor binding energy components such as the van der waal and coulombs interactions.

An accurate and efficient docking program can differentiate between the active compounds and the inactive compounds against a target from a large dataset. The authentication of a docking program can be evaluated by checking how accurately is it placing the native ligand into the binding site of the receptor protein. It is important to check the correctness while calculating thr ligand-receptor binding free energy. The correctness of the ligand placement in the binding site of the target protein is evaluated based on root mean square deviation (RMSD) between the placement of the native ligand and the placement of the docked ligand orientation. If RMSD is less than 1 Å, the quality of docking model is classified as excellent. The model is classified as good if the RMSD is greater than 1 Å and less than 2 Å and it is classified as satisfactory if RMSD is greater than 2 and less than 3 Å. However, a docking model is evaluated as bad if the RMSD is greater than 3 Å [64].

In 2015, Leonardo *et al.* analysed the molecular docking approaches that were being utilised in development of bio-active molecules (drugs) and investigated the advancements made in the disciplines related to pharmaceuticals as well as the part played in it by structural and ligand based techniques. Different strategies can be applied to improve the accuracy of molecular docking as the present scoring functions are unable to predict the absolute energy related to intermolecular interactions between novel bioactive compounds and their target receptor proteins with satisfactory accuracy [25].

Researchers following this scheme use three-dimensional structures to gather knowledge and apply it to their work known as structure-based drug design (SBDD) being applied in medicinal chemistry these days due to their extensive use in molecular interactions and energetics along with induced conformational change analysis [65].

The complications encountered with handling solvent effect, entropic effect and receptor flexibility can be minimised by planning a precise virtual screening approach that are cheaper, time-saving, and effective. This can be achieved by having concrete understanding and enough experience with basics and applied methods.

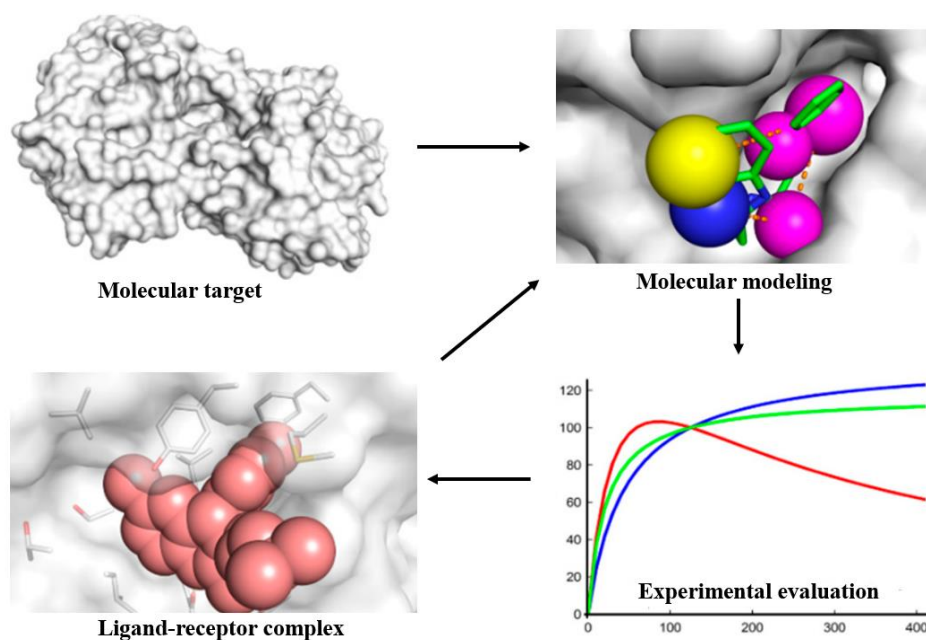


Figure 2.4 Functional process chart of structure-based drug design (SBDD)

Figure 2.4 depicts SBDD flowchart that involves three-dimensional molecular receptor structure for molecular modelling studies. These structures are used in manufacturing possible drug like bio-active compounds that are further explored through experiments. The ligand-receptor complex structures can further be utilised in designing novel compounds and modelling studies [25].

2.3.2 Ligand Based studies for uPA

Pharmacophore is considered as a three-dimensional model of the common steric and electrostatic features as described by Seidel *et al.* in 2010. The non-covalent ligand-receptor interactions are labelled as pharmacophoric features characterised for example aromatic rings, hydrophobic regions, hydrogen bond donors and hydrogen bond acceptors, cationic and anionic groups. The position and the orientation of the selected

pharmacophoric features is of utmost importance. These characteristics make a good and efficient pharmacophoric model with immaculate predictive properties that is able to portray the type of functional groups along with their precise location [66].

Mahmoud *et al.* in 2014 contributed in finding sophisticated pharmacophores using inhibitors of seven distinct sets. The chemical space of the 202 inhibitors was investigated for the retrieval of high-quality pharmacophore models that were ultimately analysed by quantitative structure-activity relationship (QSAR) based on genetic algorithm. This analysis provided a platform for evaluating the most favourable combination of physicochemical properties and pharmacophore models that can elucidate the variation within the pharmacological activity of the training set of inhibitors. According to the QSAR equation three orthogonal pharmacophoric models came out implying that there are three possible binding modes of interaction available at the binding site of the uPA. These binding modes of interaction were like the ones witnessed in the crystal structures of ligands in complex with uPA showing interactions with the binding site. The compounds available at the national cancer institute (NCI) were screened through the build pharmacophore models and generated QSAR equation which were further employed to in vitro testing. Three hits were retrieved from the list of compounds that showed better potencies as compared to existing traditional amiloride inhibitors against uPA. Pharmacophore based virtual screening incorporation with quantitative structure-activity relationship proved as a beneficial method for discovering novel uPA inhibitors of distinct nature [67].

Ligand based drug design techniques are acknowledged as computational tools applied in screening of large data sets of possible drugs like compounds. Pharmacophore modelling is one of the most frequently used technique applied in lead identification, lead optimization, selectivity profiling and compounds with possible toxic influences can be identified through ligand-receptor interactions and further explored. In 2015 Teresa *et al.* focused particularly on pharmacophore-based virtual screening of target hydroxysteroid dehydrogenases and highlighted the importance of pharmacophore modelling based on the achievements accomplished for this technique in various fields and suggested it to be utilised in future work [28].

2.3.3 Quantum mechanical studies for uPA

For drug designing of novel medications it is essential that there is molecular complementarity between the ligand and the binding site of the receptor protein through noncovalent bonds for example hydrogen bonds, hydrophobic forces, van der Waals forces, π - π interactions, and/or electrostatic effects. Consequently, in rational drug design the information on the target protein is utilised in producing novel medications[33]. In the following exemplary work presented by Christian *et al.* in 2018, the energy of interaction between the target protein urokinase type plasminogen activator and three different inhibitors was calculated through quantum mechanics-based Density Functional Theory (DFT) calculations. Three different ligands (PDB ID: 1SQA, 1SQO, and 1FV9)[68] in complex with the target protein were used in crystallographic arrangement for the quantum biochemistry calculations. The interaction energies calculated for the ligands are given in Table 2.2.

Table 2.2 *The calculated interaction energies for the three ligands UI1, UI2 and 172 with urokinase type plasminogen activator are in agreement with the theoretical results that are -107.3 kcal/mol, -99.4 kcal/mol and -35.3 kcal/mol respectively.*

Ligand	Binding energy
2-amino- 5-hydroxybenzimidazole (172)	-35.30
UI1	-107.30
UI2	-99.5

The generated results concur with the known experimental values. The ligands UI1 and UI2 showed binding interactions with uPA at binding energy level lower than -4.0kcal/mol for the following residues: ASP189, SER190, cysteine(CYS)191, glutamine(GLN)192, CYS220, TRP215, GLY216, and GLY219. However, ligand 712 showed important binding interactions with ASP189, CYS191, SER190 and CYS220 amino acid residues of the binding pocket. The distance of radius from ligand was chosen as 10 Å so that the residues showing interactions in theoretical results are examined. The mentioned work inspires the use of quantum biochemistry for the progression and development of new medications for malignancies as these theoretical approaches open the doors to comprehend the binding mechanism of the receptor protein uPA.

Literature Review

Furthermore, good correlation has been recognised between amino acid residues involved in uPA binding interactions and the significant features of ligand. For ligand UI1 the significant amino acid residues showing interactions with uPA are ASP189, CYS191-CYS220, GLN192, GLY219, SER190, GLY216, ASP60A, and TRP215 arranged in descending sequence according to interaction energy values lower than -4.0 kcal/mol paying a role in total energy. For ligand UI2, the amino acid residues sequence according to decreasing energy values is CYS191-CYS220, GILY219, ASP189, GLN192, GLY216, SER190, SER146, and TRP215. For compound 172, ASP189, CYS191-CYS220, and SER190 are depicted as the most significant residues in their decreasing order based on energy values. From the obtained results, ASP189 is a significant residue of uPA and the functional group interacting with this residue has a strong effect on the total binding energy depending upon its protonation state. According to the outcomes, it is stipulated that the naphthamide scaffold is the key factor in ligands UI1 and UI2 contributing about -48.01 kcal/mol and -62.37 kcal/mol to the total binding energy and is a crucial feature in the effectiveness of the drug like compounds. The aminopyrimidine scaffold contributes about -41.88 for UI1 and -37.03 kcal/mol for UI2, respectively. The ligand UI1 has a p-amino phenyl amide moiety substituted at 6 position due to which a decrease in the binding energy is observed and contributes about -17.50 kcal/mol. While this substitution at position 6 cannot be observed in ligand UI2 and has a naphthamide scaffold at position 6 that accepts electrons from the naphthyl ring hence decreasing its electron density. It is concluded from the above study that improved models can be designed by the amalgamation of the theoretical methods with experimental systems which are more efficient and accurate in designing highly effective inhibitors for uPA [69].

3 Methodology

Urokinase type plasminogen activator (uPA) is well known to have a role in cancer metastasis whose binding pocket is unidentified and not reported. For designing efficient sophisticated inhibitors, identification of binding pocket along with important aminoacid residues showing interactions with the test ligand is essential therefore two online protein modelling web servers are used for defining suitable binding sites with aminoacid residues showing effective interactions. The binding pocket predicted was further applied in molecular docking studies for interpreting the the residues showing strong interactions with the test ligands with high affinity. Two softwares were used for verification of the generated results that are MOE and Gold. The molecular features that are crucial in the test ligands are inferred by building a pharmacophore model using ligands as training set and chemical data obtained from online data bank as test set. The binding pocket with the features and residues obtained from these calculations are extracted through Gaussview and then subjected to DFT simulations in Gaussian.

The objectives mentioned before are accomplished one at a time by starting with the prediction of the specific binding site for urokinase type plasminogen activator (uPA) inhibitors as uPA comprises of multiple binding sites for different ligands including the two endogenic inhibitors that are plasminogen activator inhibitor-1 (PAI-1) and plasminogen activator inhibitor-2 (PAI-2). Figure 3.1 provides a flow chart that illustrates the techniques being employed in this research. The set objectives are accomplished in five steps beginning with binding pocket prediction followed by structure-based and ligand-based techniques for finding the binding interactions between the target protein and the seven test ligands as illustrated in Figure 3.1. These findings were further validated by density functional theory calculations.

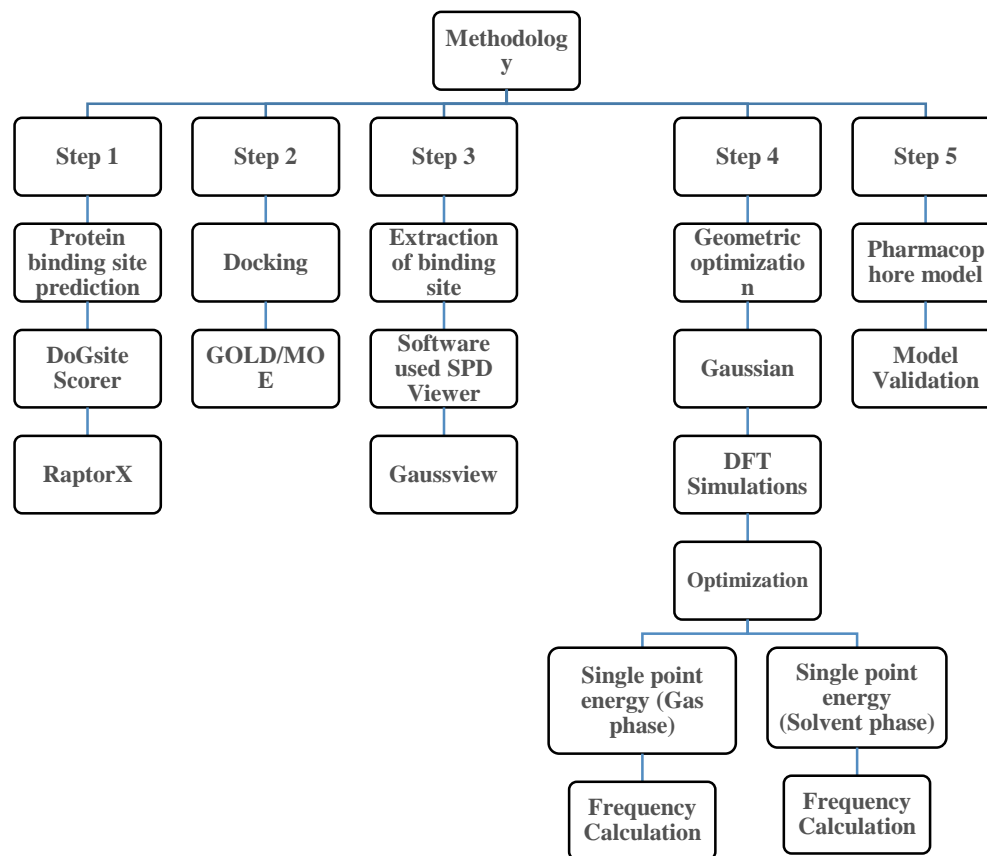


Figure 3.1 Work flow representing the steps followed to obtain the objectives of this study.

3.1 Protein binding pocket prediction

Urokinase type plasminogen activator (uPA) consists of three endogenous binding pockets for its endogenous receptor and two inhibitors, urokinase type plasminogen activator receptor (uPAR), plasminogen activator inhibitor-1 (PAI-1) and plasminogen activator inhibitor-2 (PAI-2) respectively. However, there is no work up to date that had confirmed the binding pocket for a highly potent inhibitor against uPA.

3.1.1 Retrieval of crystal structure

The structure selected for binding site prediction was obtained from PDB. The Protein Data Bank have several crystal structures for a similar protein, selecting the right one depends

upon the type of study it is being used in. The criteria upon which the crystal structure for uPA (1W10) was selected were

- The structure is in its active form with bound ligands in solvent
- The structure is present in its standard form and not the mutated protein
- The reported resolution of the crystal structure is 2.00 Å, with a lower R-factor of 0.190.
- There are no Ramachandran outliers and a low Clash score of 4.

3.1.2 uPA binding pocket prediction

DoGsite scorer and RaptorX are the two non-commercial tools used for the prediction of the binding site for uPA.

3.2 DoGsite Scorer

DoGsite scorer is an online protein modelling web server that allows the prediction of pockets and sub pockets of the target protein by the help of support vector machines (SVM). A PDB code or a PDB file is provided as an input file and provides results with up to 88% prediction correctness. These predictions are based on the search of the physico-chemical properties of the binding site and evaluates how potent is its binding affinity [70].

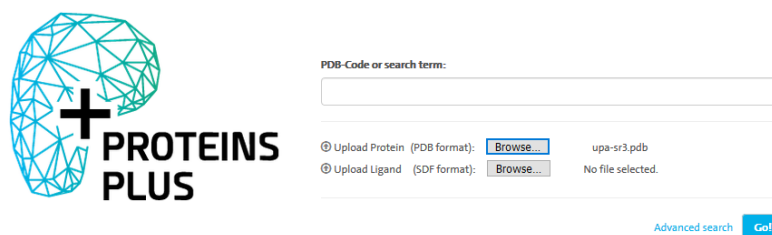
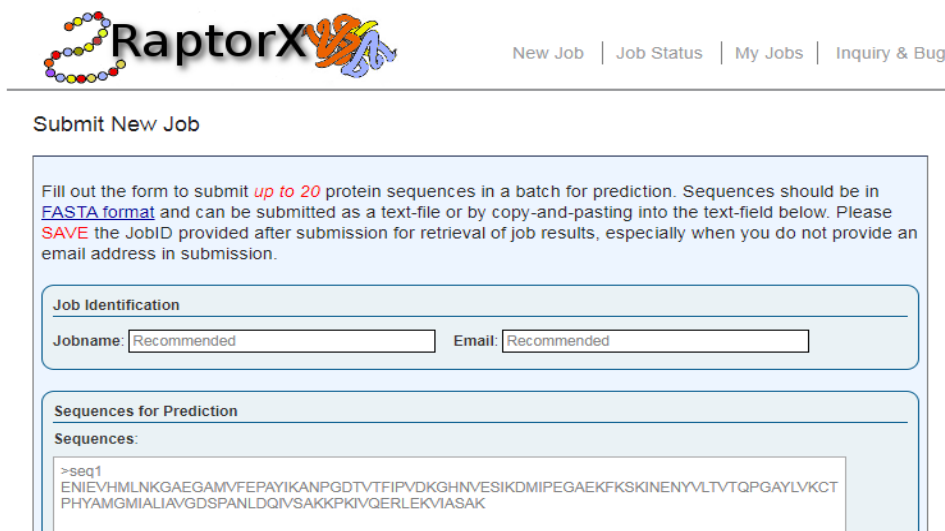


Figure 3.2 Web-Server-GUI present for DoGsite scorer for the prediction of binding sites of different proteins

3.3 RaptorX

RaptorX is a non-commercial online web portal that allows the template-based prediction of protein structures and functions utilising artificial neural networks. FASTA sequence of the protein is used as an input for the software for obtaining templates for binding site prediction.



The screenshot shows the RaptorX web portal interface. At the top left is the RaptorX logo, which consists of a colorful protein structure icon followed by the text 'RaptorX' and a stylized '3D' icon. To the right of the logo are navigation links: 'New Job | Job Status | My Jobs | Inquiry & Bug'. Below the navigation is a 'Submit New Job' section. It contains a text box with instructions: 'Fill out the form to submit up to 20 protein sequences in a batch for prediction. Sequences should be in FASTA format and can be submitted as a text-file or by copy-and-pasting into the text-field below. Please SAVE the JobID provided after submission for retrieval of job results, especially when you do not provide an email address in submission.' Below the instructions is a 'Job Identification' section with two input fields: 'Jobname: Recommended' and 'Email: Recommended'. Below that is a 'Sequences for Prediction' section with a 'Sequences:' label and a text area containing a sample FASTA sequence: '>seq1\nENIEVHMLNKGAEAMVFEPAIYKANPGDVTTFIPVDKGHNVESIKDMIPEGAEKFKSKINENVLTVTQPGAYLVKCT\nPHYAMGMIALIAVGDSPANLDQIVSAKKPKIVQERLEKVIASAK'.

Figure 3.3 Main server of RaptorX for protein structure prediction.

The predicted outcomes are sent to the provided email by the user. RaptorX predicted four binding pockets for the target protein with different multiplicity scores. The pocket with highest multiplicity score was selected as better multiplicity scores depict goodness of the predicted binding sites. Software PyMOL was used for visualising the amino acid residues occupying the predicted binding pockets. The residues were labelled as H46, D192, S193, C194, Q195, G196, S198, V216, S217, W218, G219, G221, C222 [71].

3.4 Molecular Docking

Two software tools molecular operating environment (MOE) and genetic optimization for ligand (GOLD) suit were used for docking studies. Figure 3.4 given below depicts the workflow followed for pose analysis by docking studies using the mentioned platforms.

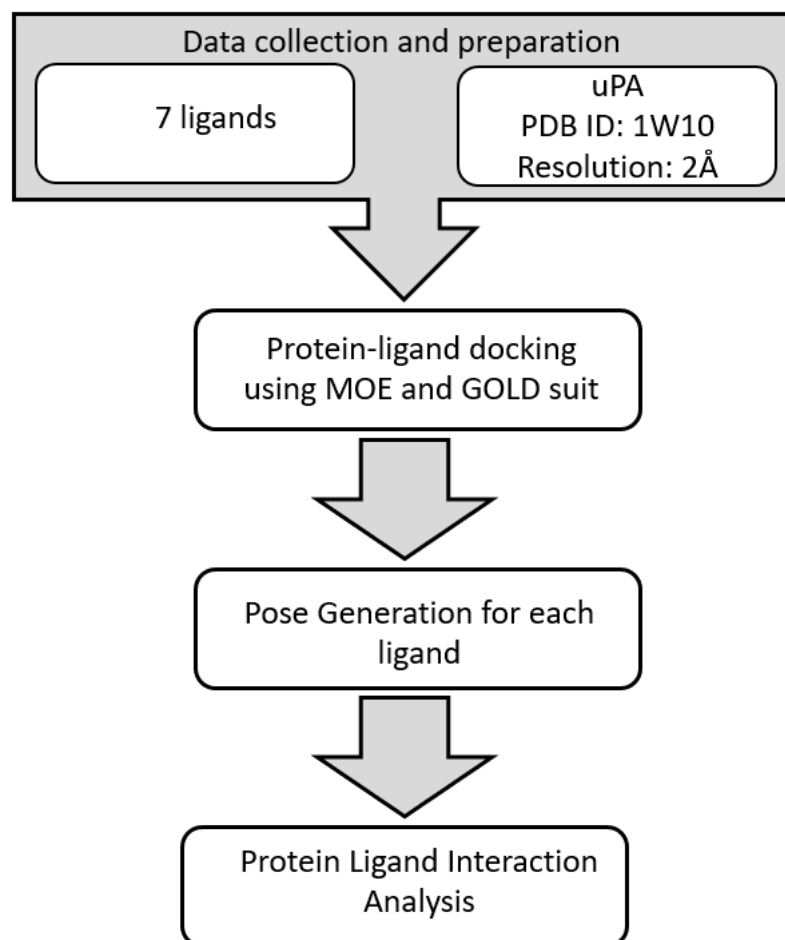


Figure 3.4 A workflow for structure based studies involving data collection and protein ligand prepared followed by docking, pose generation for each ligand and pose evaluation

MOE was used for the preparation of the ligand and protein structures. These structures were protonated and their charges were fixed, followed by energy minimisation by utilising the force field AMBER99 [72].

3.4.1 Molecular operating environment (MOE)

MOE is utilised for investigation of the binding poses of a ligand when docked into a biomolecule in three dimensional orientations. MOE was used throughout to complete the research. As the search for conformations closest to the native pose begins, only the results with lowest energies are retained in the MOE database, while the rest are rejected by the force field being used [73]. AMBER99 force field was used for the energy minimisation of the target protein uPA and the seven test ligands.

3.4.2 Genetic optimization and ligand binding (GOLD)

GOLD suit version 5.6.1 version was used for the prediction of the generated poses closest to its native binding conformation. The seven ligands under test were docked into the binding pocket of the target protein with PDB ID: 1W10 with resolution 2Å. X, Y and Z coordinated were used for the allocation of the binding site in the docking studies within 15Å radius so that all the significant amino acid residues are encompassed within the range of the binding pocket. Ten poses were generated of each ligand using the GOLD scoring function as the accuracy rate is up to 81% in the predicted poses [74]. And the generated poses were analysed through MOE for selecting the most favourable conformation based upon the binding interaction between the ligands and the residues of the binding pocket.

3.5 Active site extraction/Model

Quantum mechanical studies are very costly and exhaustive, consuming much time. Therefore, it is recommended to withdraw the binding pocket of the biomolecule that is involved in binding interactions with ligand. For the extraction of binding pocket of uPA from within the whole biomolecule, a molecular visualisation tool Swiss-Pdb viewer was used. The extracted structure was further utilized for generation of model complex geometry. Swiss-Pdb viewer is a non-commercial molecular modelling tool that provides a very user-friendly interface making it easy to visualise multiple biomolecules at the same time. This software is developed by Nicolas Guex, Alexandre Diemand, Manuel C. Peitsch, & Torsten Schwede [75].

3.6 Pharmacophore model

A pharmacophore model is a three-dimensional illustration that embodies the standard electrostatic and steric features of a protein molecule that helps predict the complementary features responsible for binding interaction between the ligand and the target protein. These interactions are responsible for the expected biological response [66]. A pharmacophore model can tell apart the actives from the inactive compounds on the base of the common electrostatic and steric features such as the hydrogen bond donors, hydrogen bond

acceptors, aromatic ring, hydrophilic and hydrophobic features. The selected features have an adjustable radius and space in angstrom (Å).

3.7 Quantum mechanical studies/calculations

The Quantum mechanical calculations were achieved by Density functional theory (DFT) method to achieve the objective of finding the binding affinity of the test ligand within the binding pocket of the target receptor protein uPA. However, QM studies can only be practised on simpler and smaller molecular structures and complexes. QM is also far truthful than the classical force [76]–[78]

3.7.1 GaussView

The input file can be generated from the GaussView graphical interface.

3.7.2 Gaussian 09

The DFT studies were carried out using a commercial software GAUSSIAN 09 that was developed by Sir John Pople in 1970. The results generated by Gaussian 09 can be observed with the help of GaussView that is also a commercial program. The input file can be generated from the GaussView graphical interface. Gaussian is used for calculating binding energies, the single point energies, SCRF and frequencies for the molecular complex [79].

3.7.2.1 Geometry Optimization/Energy Optimization

Molecules in nature exist at their lowest energy form. Energy minimisation helps in getting as close to the native structure as possible. The structures show much higher stability at lower energies levels. Hybrid function B3LYP is a vastly used functional sometimes used in combination with LANL2DZ and SDD as the basis set during the optimization of the ligand-protein complex, optimization of ligand and binding pocket without the ligand [80].

3.7.3 Frequency Calculation

Zero-point correction energies are derived by calculating the frequencies on the optimized geometries to identify that there must be no imaginary frequency exist in the energy minimized structure. Once the geometries were optimized their nuclear vibrational motion modes can also be analysed through frequency calculations. It is important to make sure that there are no imaginary frequencies or negative frequencies [81].

3.7.4 Single point Energy and Self-Consistent Reaction Field Calculation

Stuttgart Dresden (SDD) effective core potential basis set was used for the calculation of the single point energy in both the gas phase (vacuum) and the solvent phase (water) for all the optimized geometries as it generates highly accurate calculations [82]. The electronic energy of the model complex geometry is calculated as the single point energies and their SCRF calculations are also taken into consideration.

3.8 MOLDEN

Molden is a free molecular and electronic visualisation package that can read and display all the GAUSSIAN output file displaying the molecular density, molecular orbitals, electron density and atomic density. MOLDEN can be run on Windows or the OpenGL versions can also be utilised for the visualisation of output files such as chemx, PDB, Mopac (semi empirical calculations). Reference given below provides additional information

4 Results and Discussion

Urokinase type plasminogen activator (uPA) is recognized to have a part in dissemination of cancer cells and the binding pocket is unidentified for this protein and not testified. For crafting effectual inhibitors, identification of binding pocket along with main aminoacid residues showing interactions with the test ligand is necessary consequently, suitable binding sites are generated by two online protein modelling web servers that are DoSite scorer and RaptorX. The binding pocket estimated were furthered applied in molecular docking studies for interpreting the the residues showing strong interactions with the test ligands with high affinity. Two softwares were used for verification of the generated results that are MOE and Gold. The key molecular features that are in the seven ligands under test are identified by building a pharmacophore model using ligands for building training set and chemical data obtained from online data bank as test set. The binding pocket with the features and residues obtained from these calculations are extracted through Gaussview and then subjected to DFT simulations in Gaussian.

4.1 Molecular docking

Molecular docking is used for predicting protein-ligand interactions by exploring the conformations generated within the binding pocket by a ligand and was performed using the Molecular operating environment (MOE)[73] and Gold suit [83]. The results produced by considering the conformational variability and dynamics are more reliable as experiments can justify them. Before going for docking, it is essential to know the binding pocket. Two different online servers are used for the prediction of a binding pocket that is most likely to be like the original binding pocket as described. The listed docking parameters and methods are used to compare the crystallised docked complex of ligand and protein obtained from PDB. The ligand is first removed so that it can be re-docked to analyse the efficacy of the parameters by looking at the orientation of Cartesian coordinates. The difference is measured in terms of the RMSD having a threshold of 2Å as observed in the literature [83].

4.2 Binding pocket prediction

There is no distinguished binding site in Uniprot data shown for protein uPA. The literary work [6], [58], [84] present till date points towards specific amino acid residues (ASP189, SER190) that show improved potency along with selectivity towards the ligands hence minimising the off-target toxicity. However, the seven inhibitors being used are new with no related work presenting the binding site for these inhibitors. For the prediction of the binding site, two software was used:

- DoGsite scorer
- RaptorX

4.2.1 DoGsite scorer

The ligand was docked in different orientations with the protein uPA using open source pocket prediction software DoGsite scorer [85] and nine pockets with different amino acid residues and drug scores were generated. The second predicted pocket (P_1) highlighted with red having amino acid residues Alanine183 (ALA183), ALA184, ALA221, Arginine217 (ARG217), Aspartate189 (ASP189), ASP194, ASP223A, Cysteine191 (CYS191), CYS220, Glutamine192 (GLN192), Glycine (GLY216), GLY219, GLY226, Histadine99 (HIS99), Isoleucine17 (ILE17), Leucine181 (LEU181), Lysine223 (LYS223), LYS224, Proline225, (PRO225), Serine146 (SER146), SER190, SER214, Threonine147 (THR147), THR229, Tryptophan21 (TRP215), Tyrosine (TYR171), TYR172, Valine213 (VAL213), VAL227 and drug score of 0.67 as shown on the right side of Figure 4.1 was suggested to be used in further studies as it presented favourable interactions with the ligands.

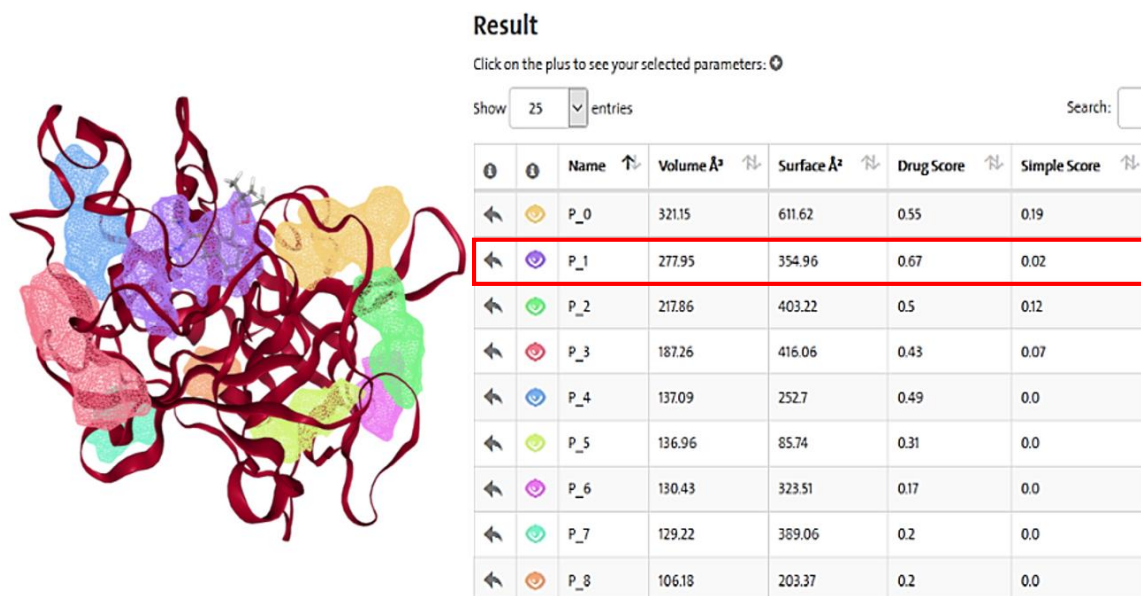


Figure 4.1 Results generated by DoGsite scorer showing nine possible binding pockets.

The left side of Figure 4.1 shows protein uPA with all the possible binding sites in different colours predicted by DoGsite scorer. The right side of the Figure 4.1 represents the pockets with respective colours along with their volume, surface area and drug scores. Predicted pocket number two (P_1) coloured with purple had all the important amino acid residues as mentioned in the literature to show increased potency and better binding with the ligands. The residues present within the different predicted pockets are mentioned in Table 4.1 given below with their calculated drug scores.

Table 4.1 Predicted binding pockets with residues and drug scores generated by DoGsitescorer.

Pocket name	Amino Acid Residues	Drug score
P_0	ARG35, ARG36, ARG37A, ASP60A, CYS41, CYS58, GLN19, GLY193, HIS237, HIS57, ILE60, PHE59, SER37, THR39, TYR40, TYR149, TYR151, TYR60B VAL38, VAL41	0.55

Results and Discussion

P_1	ALA183, ALA184, ALA221, ARG217, ASP189, ASP194, ASP223A, CYS191, CYS220, GLN192, GLY216, GLY219, GLY226, HIS99, ILE17, LEU181, LYS223, LYS224, PRO225, SER146, SER190, SER214, THR147, THR229, TRP215, TYR171, TYR172, VAL213, VAL227	0.67
P_2	ARG35, ASN74, ILE65, LEU73, LYS, THR147, TYR40, TYR149, TYR150, TYR151, VAL38	0.5
P_3	ALA184, ASP185, GLN195B, GLU137, GLY133, ILE138, LEU162, LYS161, PHE132, PRO185A, SER135, SER164, THR177, TRP186, VAL160	0.43
P_4	ARG166, CYS168, CYS182, GLN169, GLY173, HIS165, ILE163, LEU181, MET180, PHE132, SER164, SER174, THR97A, THR177, VAL176, VAL227	0.49
P_5	ALA31, ALA32, ARG70, ARG116, GLN27, GLN119, GLY69, ILE24, ILE118, LEU4, PHE30, PHE141, PRO28, SER45, THR117, TRP29, TYR40, TYR67	0.31
P_6	ARG36, ARG37A, GLU84, GLU110B, ILE65, LYS82, LYS110A, PHE82, SER110	0.17
P_7	ARG206, ASN128, GLN204, LEU123, LEU203, PRO124, SER122, SER232, THR208	0.2
P_8	ARG239, ILE47, ILE238, SER232, THR242, TRP51	0.2

The predicted binding pockets are visualised using an open source user-sponsored 3D-molecular structure visualisation tool PyMOL which is issued by Schrödinger. The atoms of the receptor protein are depicted as sticks with labelled amino acid residues as shown in Figure 4.2. The red outlined cube encloses all the amino acid residues present within the selected binding pocket (P_1).

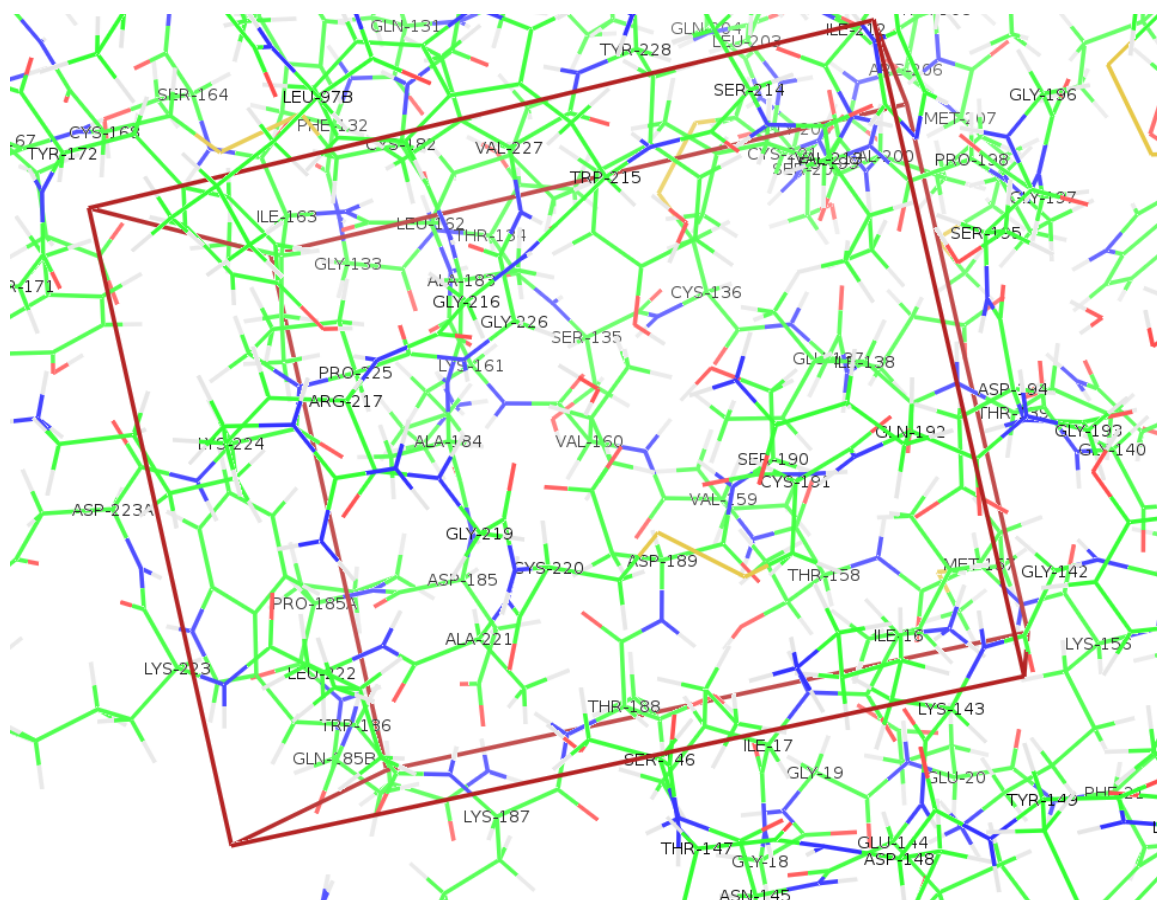


Figure 4.2 Binding pocket (P_1) predicted by DoGsite scorer. The amino acids contained in red square represent the active binding site

Green sticks represent carbon atoms, red sticks represent oxygen atoms, blue sticks represent nitrogen atoms and orange sticks represent sulphur atoms in Figure 4.2.

4.2.2 Results from RaptorX

For the validation of results obtained by DoGSite scorer, RaptorX was used for the prediction of ligand binding pocket. RaptorX produced results showing 4 different binding sites for uPA for diverse ligands. Residues differ from each other for the generated binding pockets. The multiplicity, binding residues, and the top ligands for the four predicted binding pockets are presented in Table 4.2. The pockets are analysed based on their multiplicity which is one of the confidence score that indicates the goodness of the pocket based upon the frequency with which the pocket appeared in the template structure. The first predicted pocket with highest multiplicity 127 has the amino acid residues (H46, D192, S193, C194, Q195, G196, S198, V216, S217, W218, G219, G221, C222) was most

Results and Discussion

favourable for inhibition of uPA as suggested in the literature [6], [58], [84], the selected binding pocket are presented in Figure 4.3

Table 4.2 Predicted binding pockets with their multiplicity, top ligands and binding residues generated by RaptorX

POCKET	MULTIPLICITY	TOP LIGAND	BINDING RESIDUES
1	127	SO4	H46, D192, S193, C194, Q195, G196, S198, V216, S217, W218, G219, G221, C222
2	55	SO4	H95, T178, K180, M181
3	44	CIT	R21, K75, K106
4	28	SO4	R20, H22, R23

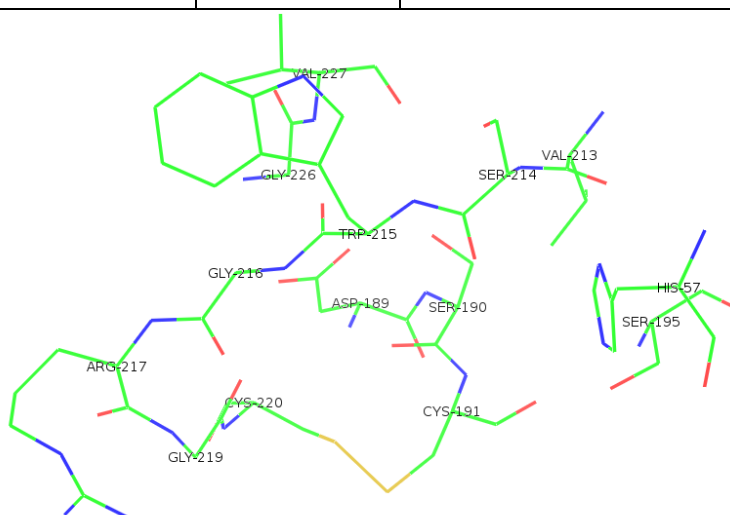


Figure 4.3 Selected binding pocket with multiplicity calculated as 127 generated with RaptorX. The amino acid residues depicted as sticks present in the pocket are labelled.

4.2.3 Analysis of generated pockets

On comparing the results obtained from both the software it was observed that the results were coinciding, had common amino acid residues (Figure 4.4). Also there are certain amino acids which are present in predicted binding site from one software are reported that were mentioned in previous studies and have influence on the selectivity as well as the potency of the ligand.

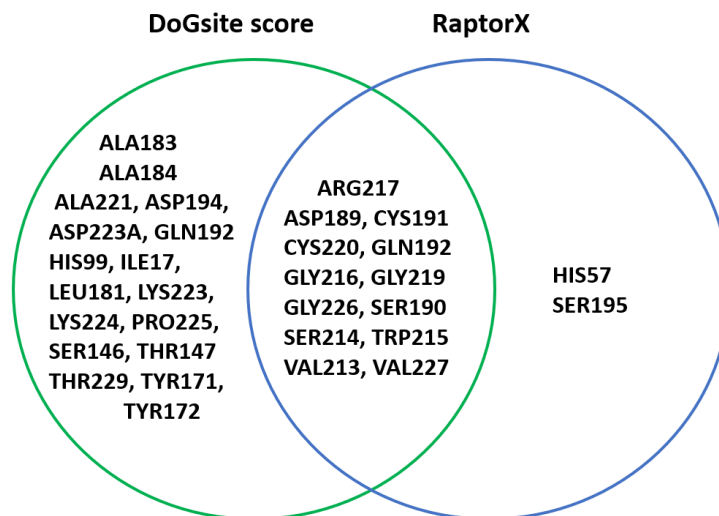


Figure 4.4 The common and uncommon amino acid residues in binding pockets predicted by DoGsite scorer and RaptorX

Figure 4.4 shows a Venn diagram that depicts the amino acid residues selected by DoGsite scorer in green circle while the amino acid residues selected by RaptorX are shown in blue circle. The common residues are ARG217, ASP189, CYS191, CYS220, GLN192, GLY216, GLY219, GLY226, SER190, SER214, TRP215, VAL213, VAL227.

After selection of the binding pocket, it was unclear how the substrate would bind to the binding pocket and in which orientation so that would maximise the favourable interactions and minimise the total energy of the ligand and protein complex. Molecular Docking technique followed by DFT was chosen to meet these objectives.

4.3 Molecular Docking

4.3.1 MOE Results

While utilising docking technique, the amino acid residues considered important in the binding pocket of uPA are as following ASP189, SER190, GLY219. For every ligand being studied, 10 conformations were generated using scoring function as LondonDG and placement method as Alpha triangle. The interactions observed within the binding pocket were saved in the form of pictures with their binding affinity energy values given as scores in kcal/mol unit. As observed in the literature the more negative the binding affinity value the better. The seven ligands showed interactions with different amino acid residues in the

Results and Discussion

binding pocket of uPA with different scores. Seven ligands BC11, BC57, AB11, AB5, JS67, JS62 and SR3 were docked in protein of interest uPA with different scores.

BC11 was docked in uPA with 10 generated conformations. The third generated conformation showed the best score -3.3591 kcal/mol along with best interactions within the binding pocket. One of the OH groups showed interaction with the residue ASP189, the Sulphur present in the ligand BC11 shows interaction with SER214 and NH₂ group shows interaction with HIS57 as represented in the 2D illustrations below Figure 4.5. The right-side image represents the 3D protein in ribbon form while the ligand is in purple ball and stick form.

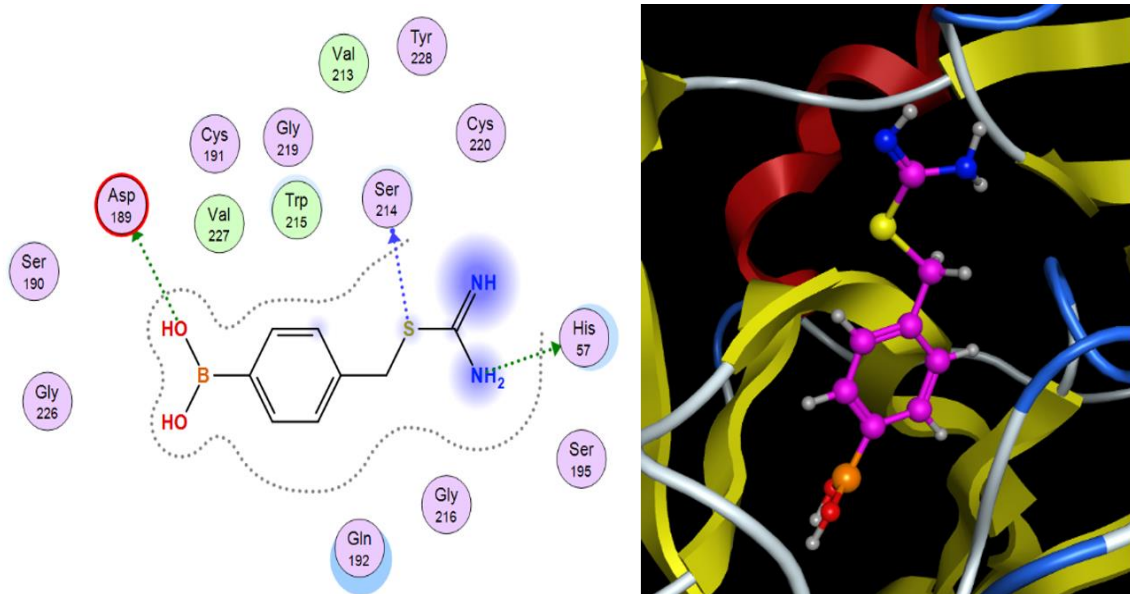


Figure 4.5 Visual representation of ligand BC11 docked in uPA binding pocket. Left image depicts the 2D representation of interactions. The right image depicts the 3D representation of ligand protein complex after docking.

BC57 was docked in uPA with 10 generated conformations. The first conformation showed the best score -4.4899 kcal/mol along with best interactions within the binding pocket. The two OH groups showed interaction with the residues HIS57 and SER214, NH₂ group shows interaction with SER146 and GLN192 and NH group of the ligand showed interaction with ARG217 as represented in the 2D illustrations below in Figure 4.6. The right-side image represents the 3D visualisation with protein in ribbon form while the ligand is in purple ball and stick form.

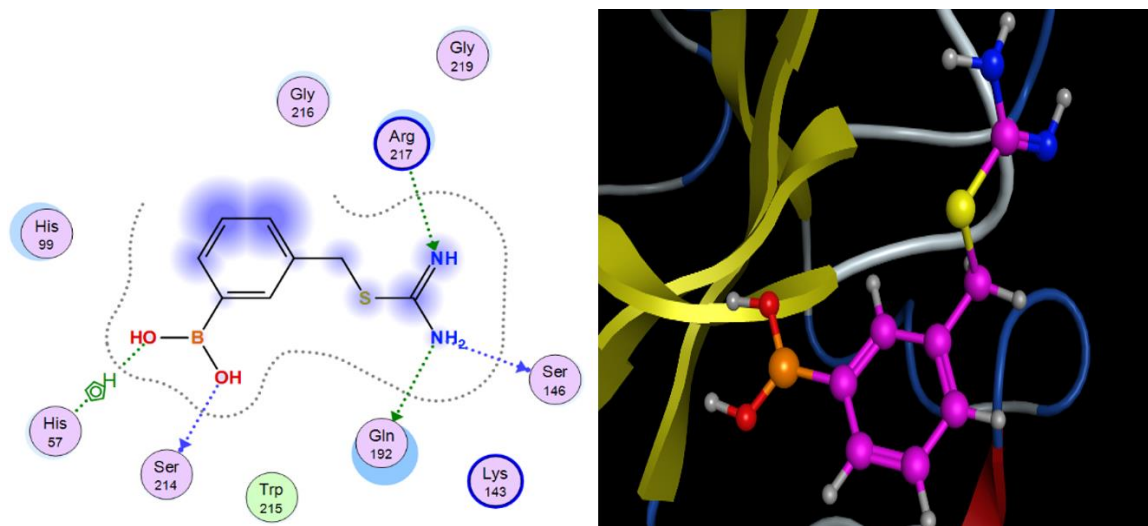


Figure 4.6 Visual representation of ligand BC57 docked in uPA binding pocket. Left image depicts the 2D representation of interactions. The right image depicts the 3D representation of ligand protein complex after docking.

JS62 was docked in uPA with 10 generated conformations. The first conformation showed the best score -5.3983 kcal/mol. Only the NH group showed interaction with ARG217 within the binding pocket as represented in the 2D illustrations given below in Figure 4.7. The right-side image represents the 3D protein in ribbon form while the ligand is in the ball and stick form.

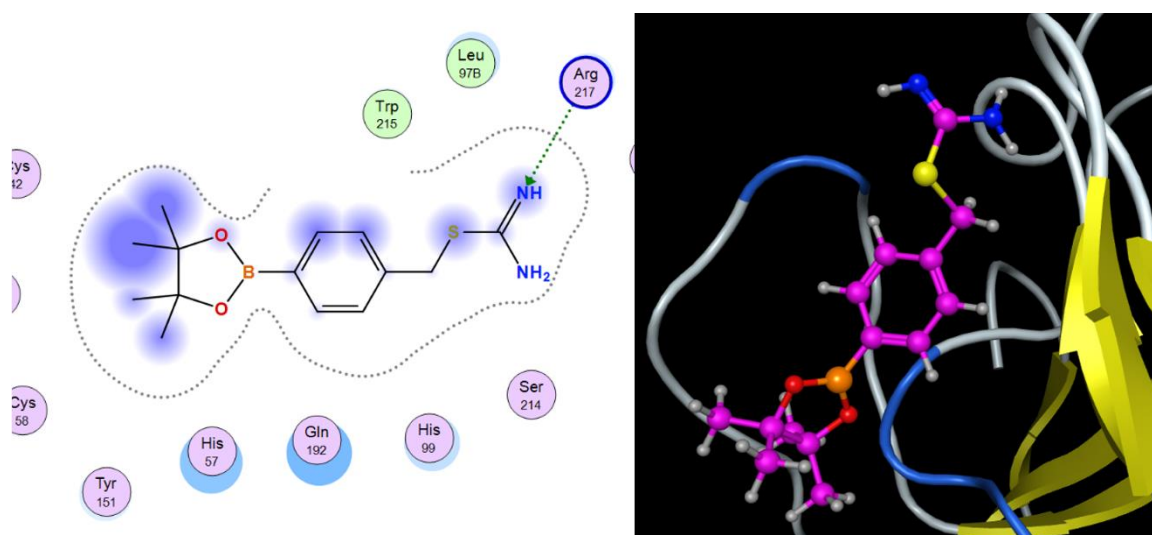


Figure 4.7 Visual representation of ligand JS62 docked in uPA binding pocket. Left image depicts the 2D representation of interactions. The right image depicts the 3D representation of ligand protein complex after docking

JS67 was docked in uPA with 10 generated conformations. The first conformation showed the best score -3.7709 kcal/mol. The Sulphur group showed interaction with the residue

Results and Discussion

ASP189, and the NH₂ group showed interaction with GLY219 and SER190 as represented in the 2D illustrations below Figure 4.8. The right-side image represents the 3D protein in ribbon form while the ligand is in purple ball and stick form.

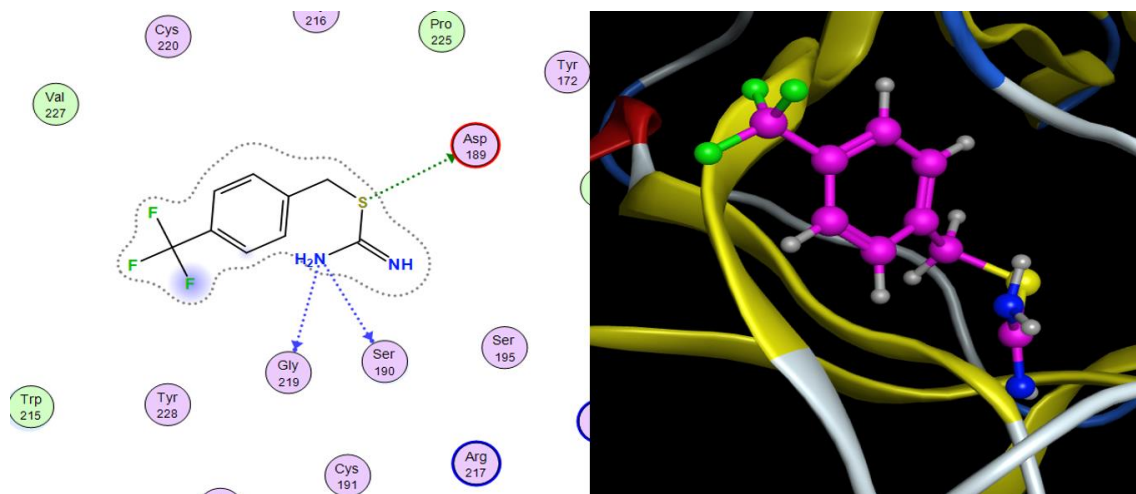


Figure 4.8 Visual representation of ligand JS67 docked in uPA binding pocket. Left image depicts the 2D representation of interactions. The right image depicts the 3D representation of ligand protein complex after docking.

SR3 was docked in uPA with 10 generated conformations. The first conformation showed the best score -3.2481 kcal/mol along with best interactions within the binding pocket. The Sulphur present in the ligand SR3 shows interaction with GLY219 and the NH₂ group shows interaction with ASP189 and SER190 as represented in the 2D illustrations below Figure 4.9. The right-side image represents the 3D protein in ribbon form while the ligand is in purple ball and stick form.

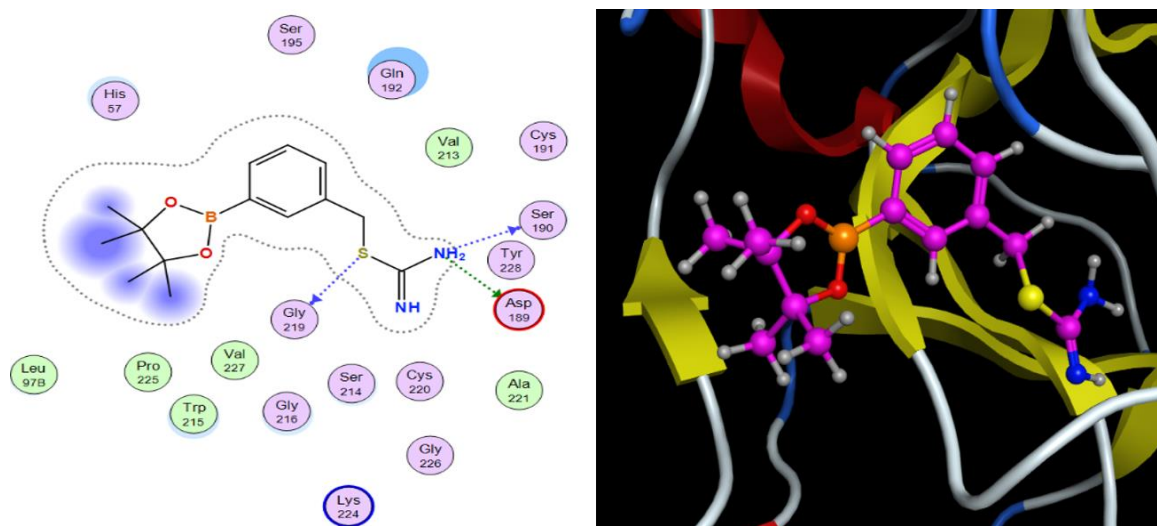


Figure 4.9 Visual representation of ligand SR3 docked in uPA binding pocket. Left image depicts the 2D representation of interactions. The right image depicts the 3D representation of ligand protein complex after docking

AB11 was docked in uPA with 10 generated conformations. The first conformation showed the best score -4.8438 kcal/mol showing no favourable interactions within the binding pocket. The Sulphur present in the ligand AB11 shows interaction with GLY219 and ARG217 and the NH group also shows interaction with ARG217 as represented in the 2D illustrations below Figure 4.10. The right-side image represents the 3D protein in ribbon form while the ligand is in purple ball and stick form.

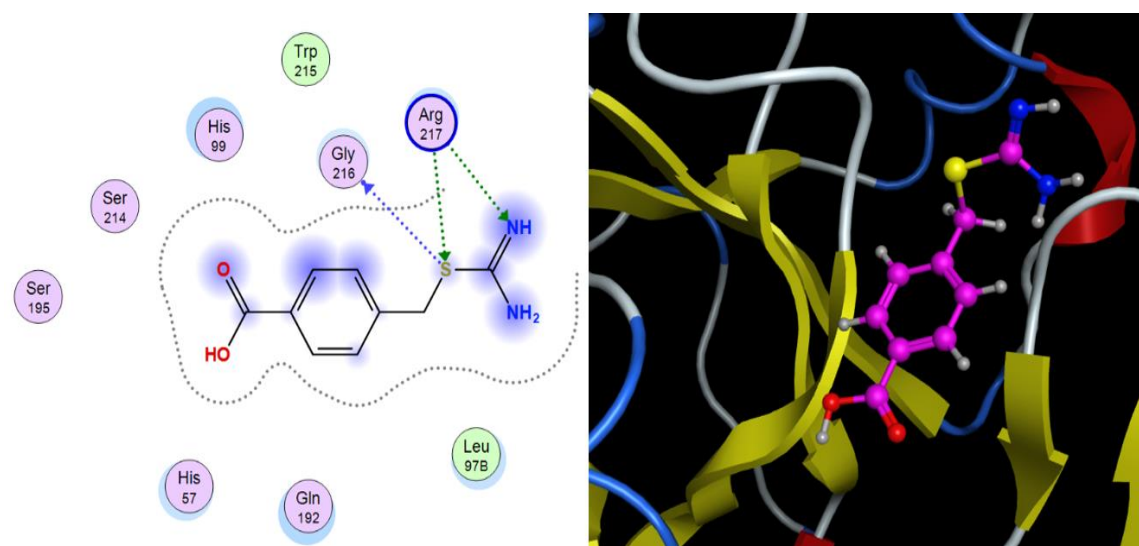


Figure 4.10 Visual representation of ligand AB11 docked in uPA binding pocket. Left image depicts the 2D representation of interactions. The right image depicts the 3D representation of ligand protein complex after docking.

Results and Discussion

AB5/4 was docked in uPA with 10 generated conformations. The third conformation showed the best score -4.6038 kcal/mol. The Oxygen functional group shows interactions within the binding pocket with ARG217 and the Benzene ring shows interactions with GLY216 as represented in the 2D illustrations below Figure 4.11. The right-side image represents the 3D protein in ribbon form while the ligand is in purple ball and stick form.

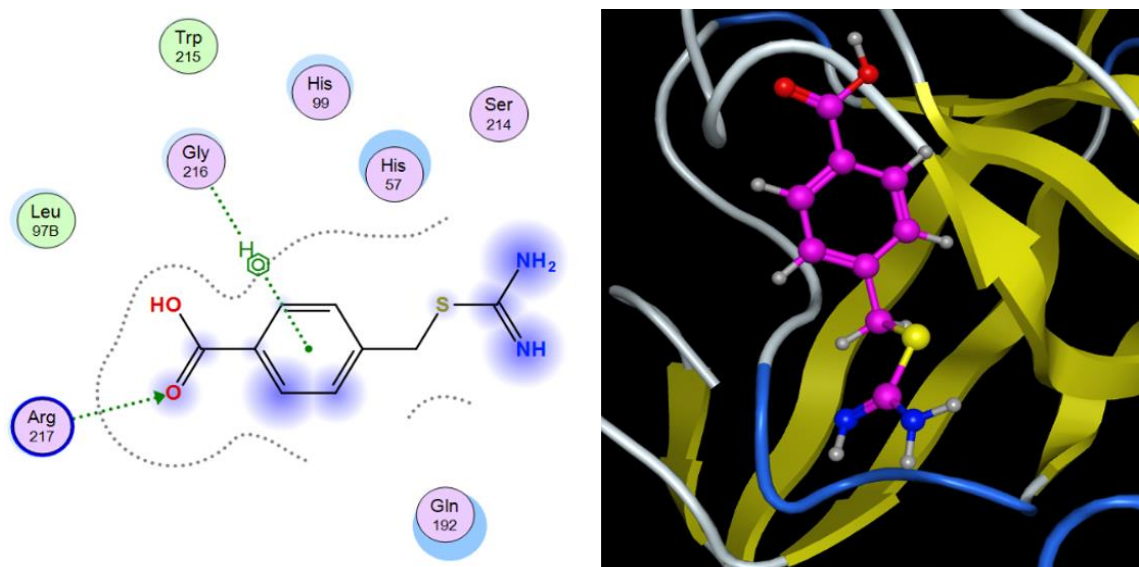


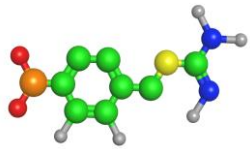
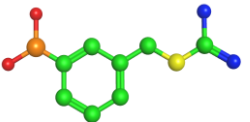
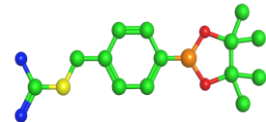
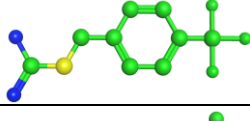
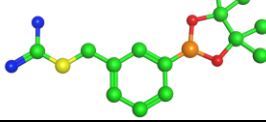
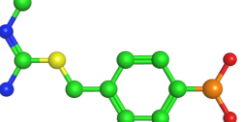
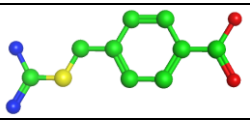
Figure 4.11 Visual representation of ligand AB5/4 docked in uPA binding pocket. Left image depicts the 2D representation of interactions. The right image depicts the 3D representation of ligand protein complex after docking

Two compounds BC11 and SR3 were carefully chosen for further analysis for density functional theory studies as they showed favourable interactions within the binding pocket as a drug like compound reveals its action only when it binds to its receptor specific binding site. It was also revealed from previous wet lab studies by performing cell viability test that four compounds JS62, JS67, AB11 and AB5/4 caused cell death when Dictyostelium cell were subjected to acute and prolonged exposure with the test compounds. Although BC57 did not cause cell death, it did not show any favourable interactions within the binding pocket.

Table 4.3 provides the structures of the seven test compounds along with their scores that is the binding free energy (kcal/mol), electrostatic interaction energy (kcal/mol) and their van der wall interaction energy (kcal/mol) within the binding pocket of the protein of interest uPA.

Results and Discussion

Table 4.3 Structures of the test ligands are given below in the form of ball and stick with the selected conformation from docking results. Binding free energy, electrostatic interaction energy and van der wall interaction energy is given in Kcal/mol

Ligand name	Ligand Structure as depicted in MOE	Conformation No.	Binding Free Energy (Kcal/mol)	Electrostatic Interaction Energy (Kcal/mol)	Van der Wall Interaction Energy (Kcal/mol)
BC11		3	-3.3591	-92.6314	5.8779
BC57		1	-4.4899	-96.0586	4.0621
JS62		1	-5.3983	-86.0209	6.8424
JS67		1	-3.7709	-52.7372	4.4346
SR3		1	-3.2481	-86.6706	12.9146
AB11		1	-4.8438	-65.9904	4.5426
AB5/4		3	-4.6038	-71.2074	4.7132

4.3.2 GOLD Results

Molecular docking was performed using GOLD suit to verify the results obtained from MOE and each pose was generated using stochastic scoring function GOLD fitness score. 10 poses were generated for each test compound.

BC11 was docked in uPA with 10 generated conformations. The first conformation was suggested as the best fit solution with score 58.3489 along with favourable interactions

Results and Discussion

within the binding pocket. The NH_2 group showed interaction with ASP189 and Lys224 and the Sulphur atom present in the test compound BC11 showed interaction with TRP215 as represented in the 2D illustrations below Figure 4.12. The right-side image represents the 3D protein in ribbon form while the ligand is in aqua stick form.

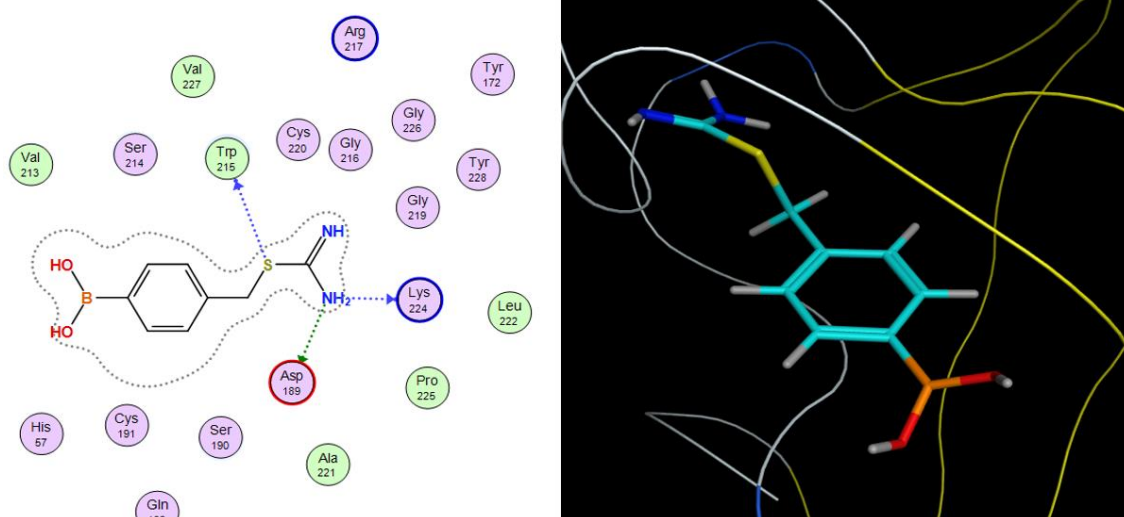


Figure 4.12 Visual representation of ligand BC11 docked in uPA binding pocket. Left image depicts the 2D representation of interactions. The right image depicts the 3D representation of ligand protein complex after docking

BC57 was docked in uPA with 10 generated conformations. The second conformation was suggested as the best fit solution with score 65.1328 along with favourable interactions within the binding pocket. The NH_2 group showed interaction with ASP189, ARG217, LYS224 and the Sulphur atom present in the test compound BC57 shows interaction with TRP215 as represented in the 2D illustrations below Figure 4.13. The right-side image represents the 3D protein in ribbon form while the ligand is in the aqua stick form.

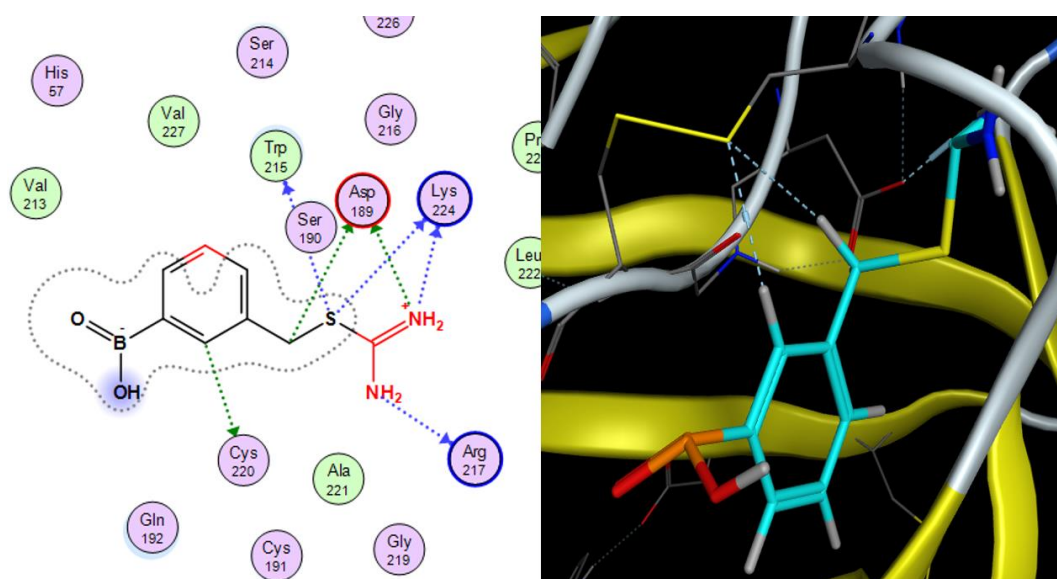


Figure 4.13 Visual representation of ligand BC57 docked in uPA binding pocket. Left image depicts the 2D representation of interactions. The right image depicts the 3D representation of ligand protein complex after docking.

JS62 was docked in uPA with 10 generated conformations. The first conformation was suggested as the best fit solution with score 47.9117 along with no favourable interactions within the binding pocket. The NH_2 group showed interaction with TRP215 as represented in the 2D illustrations on the left side in Figure 4.14 given below. The right-side image represents the 3D protein in ribbon form while the ligand is depicted in the aqua stick form.

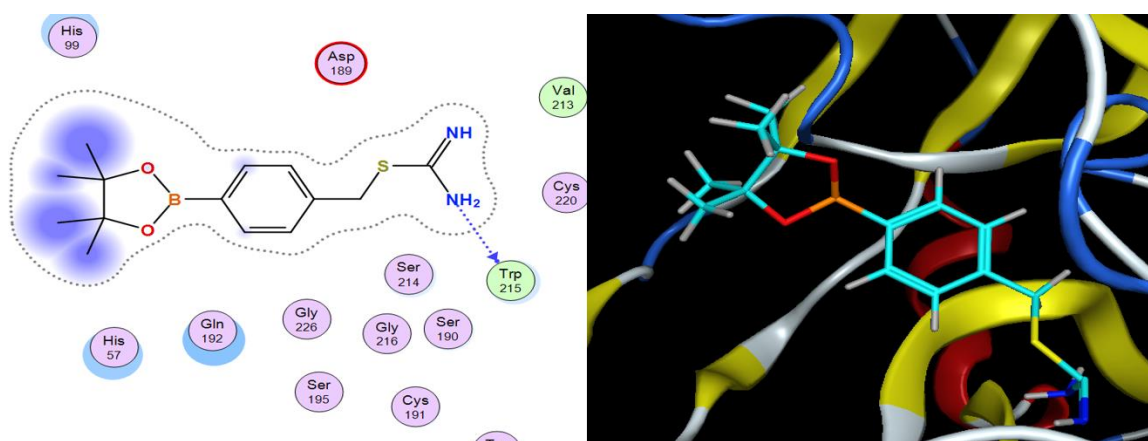


Figure 4.14 Visual representation of ligand JS62 docked in uPA binding pocket. Left image depicts the 2D representation of interactions. The right image depicts the 3D representation of ligand protein complex after docking.

JS67 was docked in uPA with 10 generated conformations. The first conformation showed the best fit solution with score 57.0528 along with best interactions within the binding

Results and Discussion

pocket. The Sulphur present in the ligand JS67 shows interaction with ASP189 and TRP215 as represented in the 2D illustrations on the left side in Figure 4.15 given below. The right-side image represents the 3D protein in ribbon form while the ligand is depicted in aqua stick form.

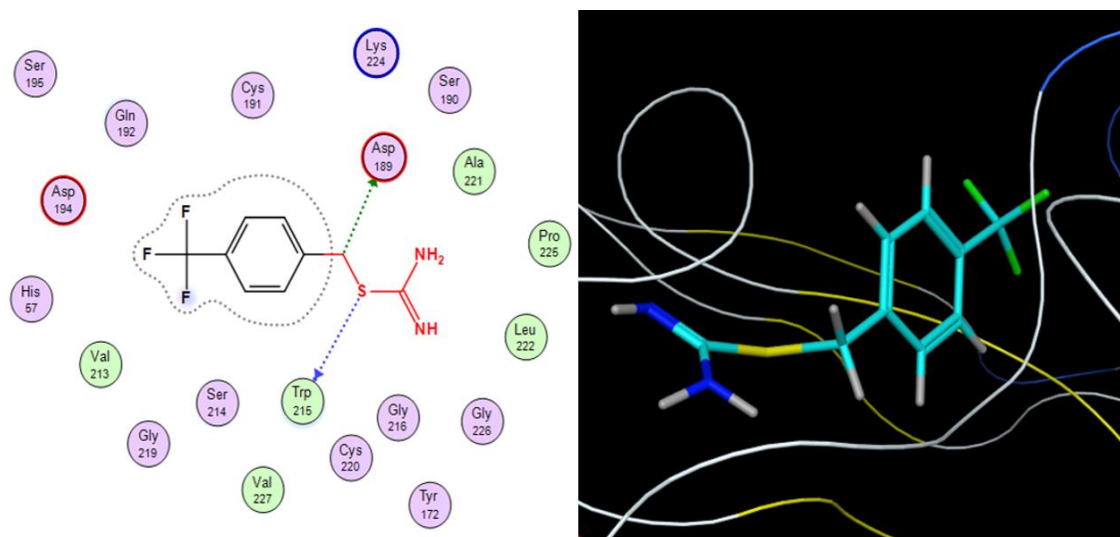


Figure 4.15 Visual representation of ligand JS67 docked in uPA binding pocket. Left image depicts the 2D representation of interactions. The right image depicts the 3D representation of ligand protein complex after docking

SR3 was docked in uPA with 10 generated conformations. The fourth conformation showed the best fit solution with score 46.4523 along with best interactions within the binding pocket. The Sulphur present in the ligand SR3 shows interaction with GLY219, the NH group shows interactions with the GLY216 of the binding pocket and NH₂ group showed interactions with ASP189 of the binding pocket as represented in the 2D illustrations on the left side in Figure 4.16 given below. The right-side image represents the 3D protein in ribbon form while the ligand is depicted in aqua stick form.

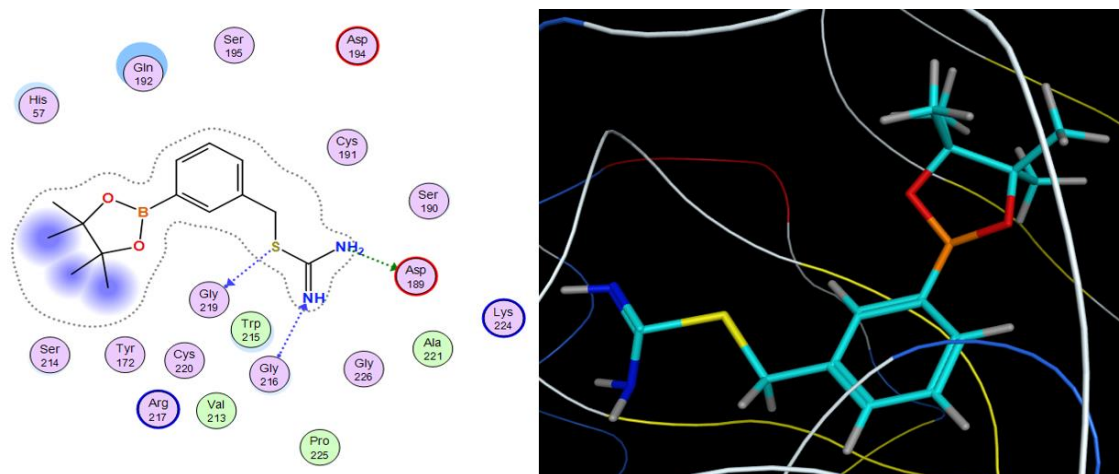


Figure 4.16 Visual representation of ligand SR3 docked in uPA binding pocket. Left image depicts the 2D representation of interactions. The right image depicts the 3D representation of ligand protein complex after docking

AB11 was docked in uPA with 10 generated conformations. The first conformation showed the best fit solution with score 53.7381. However, the test compound does not show any favourable interactions within the binding pocket. The OH present in the ligand AB11 shows interaction with SER190 as represented in the 2D illustrations on the left side in Figure 4.17 given below. The right-side image represents the 3D protein in ribbon form while the ligand is depicted in aqua stick form.

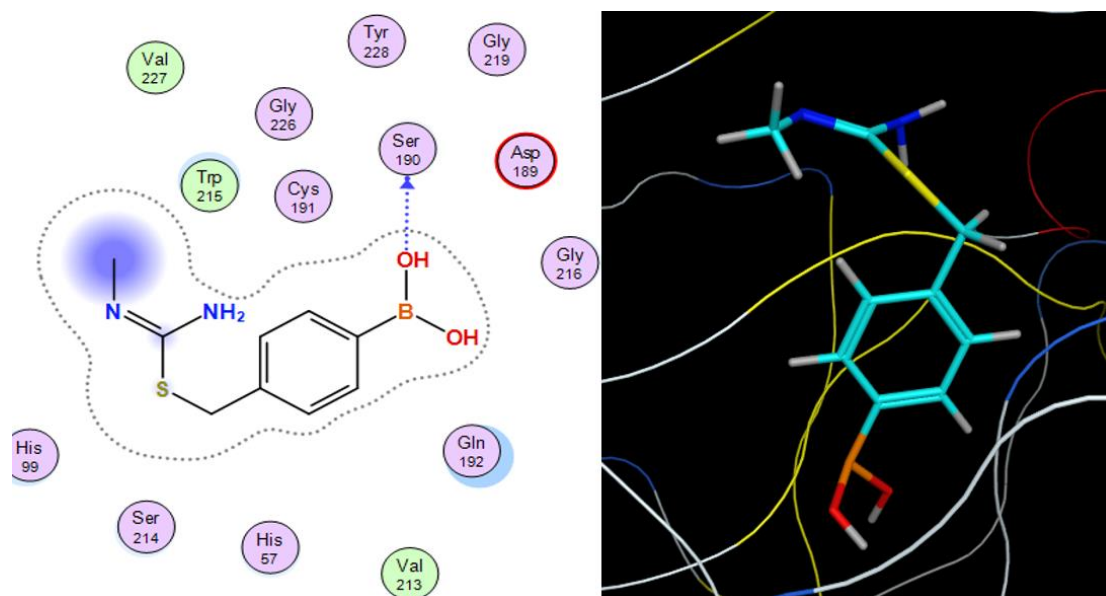


Figure 4.17 Visual representation of ligand AB11 docked in uPA binding pocket. Left image depicts the 2D representation of interactions. The right image depicts the 3D representation of ligand protein complex after docking.

Results and Discussion

AB5/4 was docked in uPA with 10 generated conformations. The fifth conformation showed the best fit solution with score 21.2873. However, the test compound does not show any favourable interactions within the binding pocket. The OH present in the ligand AB5/4 shows interaction with SER214 and Sulphur showed interactions with ArRG217 as represented in the 2D illustrations on the left side in Figure 4.18 given below. The right-side image represents the 3D protein in ribbon form while the ligand is depicted in aqua stick form.

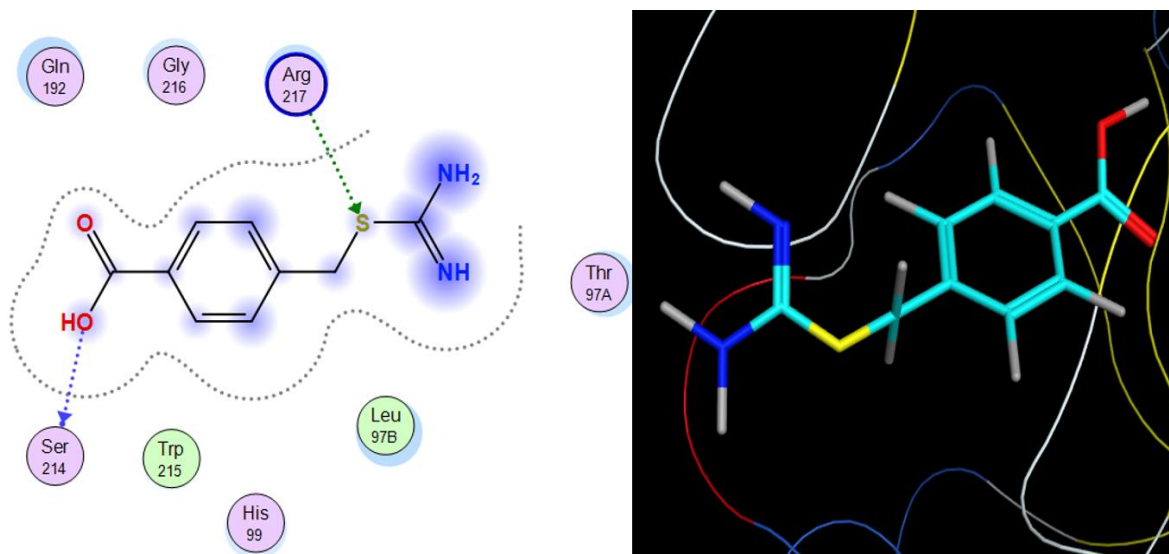
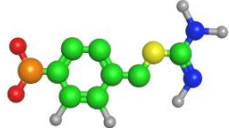
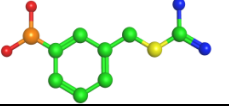
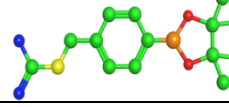
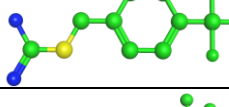
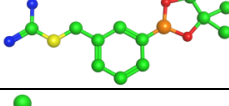
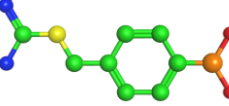
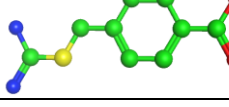


Figure 4.18 Visual representation of ligand AB11 docked in uPA binding pocket. Left image depicts the 2D representation of interactions. The right image depicts the 3D representation of ligand protein complex after docking

Table 4.4 enlists the seven test compounds along with their structures. The conformations selected for further analysis are also mention along with the calculated binding free energy (kcal/mol) as Gscore.

Results and Discussion

Table 4.4 Table representing test compound structures in ball and stick figures along with their generated score through scoring function Gold score

Ligand name	Ligand Structure as depicted in MOE	Conformation No.	Binding Free Energy (Kcal/mol)
BC11		1	58.3489
BC57		2	65.1328
JS62		1	47.9117
JS67		1	57.0528
SR3		4	46.4523
AB11		1	53.7381
AB5/4		5	21.28

4.3.3 Validation and accuracy

Two software were used to validate the accuracy of the results generated through docking. For each ligand docked in uPA, 10 poses were generated using scoring function LondonDG in combination with Alpha triangle as the placement method. The binding affinity calculated for the ligands BC11, BC57, JS62, JS62, SR3, AB11, AB5/4 are -3.3591, -4.4899, -5.3983, -3.7709, -3.2481, -4.8438, -4.6038 respectively. Even though JS62, AB11, AB5/4 shows the highest fitness score, they are not selected for further studies as previous studies (Rafiq,2015) reports cell apoptosis caused by JS62, JS67, AB11 and AB5/4. Therefore, these ligands will not be mentioned in the quantum mechanical studies.

Results and Discussion

The criteria for selection of promising ligand candidate is the binding conformation rather than the fitness score. SR3 showed binding interactions with the important amino acid residues ASP189, SER190 and GLY216 in the previous studies (Rehman,2018) and when compared to the generated results it is observed that amino acid residues ASP189, SER190 were common.

Additionally, the contribution of SER190 in the binding of uPA with the drug like molecules within the S1 binding sub-site was evaluated by Katz *et al.* and co-workers in 2004 when they studied the binding of inhibitors with uPA that had a mutated side chain at position 190 comprising an Alanine residue instead of Serine. An 18-fold decline was recorded for the dropped potency for two lead compounds 5-amidinobenzimidazole and 5-amidinoindole while a 12-fold decline for the compounds 2-amino-benzamidazole and aryl-guanidine was recorded by applying enzymology and a diverse crystallographic data set of proteases in complex with the selected inhibitors. It was concluded that the drug effectiveness and selectivity was highly influenced by the hydroxyl group present within the SER190 residue and the deficiency had a negative effect on the overall performance. On further experimentation, it was realised that when 6-halo group substitution was carried out for the compound 5-amidinoindol the selectivity was boosted up to 170-folds over the alanine(ALA)190 mutant designed for uPA ($K_i = 14\text{nM}$) and for ALA190 in tPA it showed an increase of 630-fold. Interestingly, fluoro-5-amidinobenzimidzole ($K_i = 11\text{nm}$) that is a lead compound showed a 1000-fold and a 100-fold upsurge in selectivity against uPA as compared to the rest of the proteases with residues ALA190 and SER190 individually. This alone highlighted the importance of SER190 residue at the position under thought in the effective inhibition and potency. This amplification in the selectivity can be scrutinised in detail on the structural basis by regarding the differences between various inhibitor-bound protease complexes. There resides a conserved water molecule in the binding pocket of uPA at S1 sub-site that is locked in place during the binding of inhibitor to the uPA in absence of the hydroxyl group in the mutated uPA-SER190Ala. However, integration of the 6-halo group dislocates this water molecule as a result permitting direct and deeper inhibition by forming hydrogen bond between the inhibitor and SER190 residue of the uPA.

Results and Discussion

Docking results obtained by using GOLD suit are presented in 4.2.3 in Chapter 3. For each of the seven ligands 10 poses were generated using fitness score GOLD to score each generated pose. The score calculated for the ligands BC11, BC57, JS62, JS62, SR3, AB11, AB5/4 are 58.3489, 65.1328, 47.9117, 57.0528, 46.4523, 53.7381 and 21.28, respectively. Again, the criteria for selection of a promising ligand is not the fitness score but amino acid residues involved in the binding interactions.

Figure 4.19 given below, compares the amino acid residues showing binding interactions with uPA binding pocket through docking using two software and the previous studies for three ligand BC11, BC57 and SR3, respectively. It can be observed from Figure 4.5 that shows binding interactions of ASP189 with the hydroxyl group (OH) of the ligand BC11 using MOE. However, Figure 4.11 shows binding interaction between ASP189 and the amine group (NH_2) of the ligand BC11 while using another software GOLD for docking studies. From the results presented above, it can be seen in Figure 4.6 that BC57 does not show commonality in binding interaction with the two important residues ASP189 and SER190. Hence, finally SR3 was the only ligand used for quantum mechanical studies as they are very time consuming and computationally expensive.

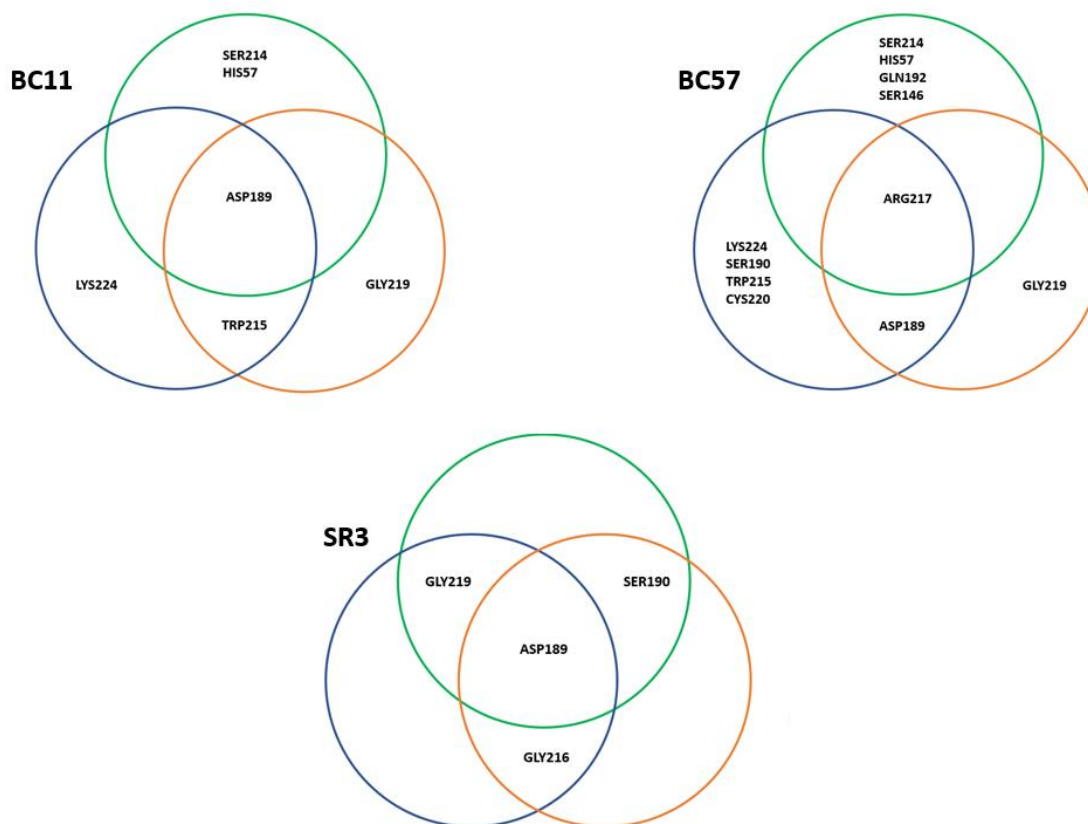


Figure 4.19 Green circle represents results obtained from MOE. Blue circle represents results obtained from GOLD. Orange circle represents results obtained from the previous studies. The three diagrams depict the amino acid residues for three ligands BC11, BC57 and

4.3.4 Pharmacophore modelling

Pharmacophore model was generated using molecular operating environment (MOE). The intention for building a pharmacophore model was to show a concept which explains the importance of different selected pharmacological features in the test compounds and not to optimize the inhibitory effect of these test compounds that act as inhibitors.

4.3.5 Template selection

For the seven test compounds against the target protein uPA, all seven are chosen as template for generating pharmacophore model based on their high potency and selectivity. The compounds were aligned by flexible alignment method and used as template for random selection of favourable pharmacophoric features.

4.3.6 Selection of test set and activity Cut-off

263 boronic acid derived inhibitors against uPA in humans with known IC_{50} values were selected from Binding database (BDB). Compounds with unknown IC_{50} values were removed from the test set. Furthermore, the seven test compounds had IC_{50} values lower than $69\mu\text{M}$ which makes them fitting for activity cut-off. The compounds in the test data with $69\mu\text{M}$ were considered as active compounds while the compounds above $69\mu\text{M}$ were considered as inactive compounds. Out of total 263 compounds, 63 lies in the active compounds which have IC_{50} values equal to or less than $69\mu\text{M}$ and 200 compounds lies in the inactive compounds which have IC_{50} values greater than $69\mu\text{M}$ which is the cut-off value as stated before.

4.3.7 Query generation

For the target protein uPA pharmacophore queries were generated by using MOE software. The model was built through random selection of the different pharmacophoric features and removal of those descriptors that had no effect on the differentiation of active from inactive. The selected pharmacophoric features were revised through modifications or by altering the Gaussian radius so that maximum number of actives can be selected as hits by the generated pharmacophoric model.

4.3.8 Model evaluation

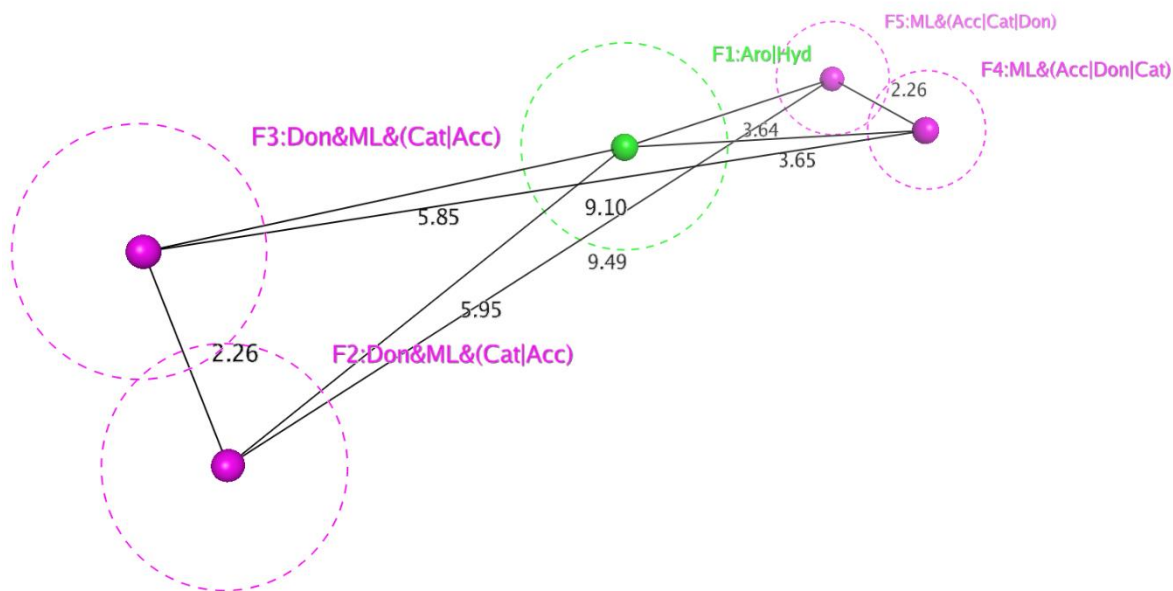


Figure 4.20 Statistically significant (19% True positive and 59.3% True negative rate) boronic acid derivative inhibitors pharmacophore model obtained using docking conformations of seven inhibitors aligned with flexible alignment used as a template. The pharmacophore consists of four cationic hydrogen bond acceptors and two cationic hydrogen bond donors with one aromatic ring.

The pharmacophore model for the seven ligand was 78% accurate suggesting that the generated model in this analysis is well-predicted making it efficient in distinguishing between active and inactive compounds which indicates it is able to classify actives as hits selectively. In conclusion, the model is finalised for the selected test set of 263 compounds (as shown in Figure 4.20) that was able to select all active compounds as hits except for 13 active compounds. The pharmacophore model selected for screening the boronic acid derivative inhibitors of uPA comprises of five distinct features that are:

- F1 Aromatic hydrophobic ring (Aro-Hyd),
- F2 Hydrogen bond donor and metal ligator and cation hydrogen bond acceptor [Don&ML&(Cat|Acc)],
- F3 Hydrogen bond donor and metal ligator and cation hydrogen bond acceptor [Don&ML&(Cat|Acc)],

Results and Discussion

- F4 Metal ligator and hydrogen bond acceptor and cation and hydrogen bond donor [ML&(Acc|Cat|Don)],
- F5 Metal ligator and hydrogen bond acceptor and cation and hydrogen bond donor [ML&(Acc|Cat|Don)].

These selected pharmacophoric features have radius within the range of 1.0-2.0 Å. Table 4.5 given below presents the distances calculated among the pharmacophoric features of the ligand data set. The sensitivity and specificity were also calculated for the generated pharmacophore model which signifies the correctness of the model. By putting the values within the present equations, the following solutions were generated:

Table 4.5 Calculated distance between the features of pharmacophore model.

Feature		F1	F2	F3	F4	F5
Aro Hyd	F1	0	5.95	5.85	3.65	3.64
Don&Acc2	F2	5.95	0	2.26	8.94	9.49
Don&ML&(Cat Acc)	F3	5.85	2.26	0	9.10	9.49
ML&(Acc Don Cat)	F4	3.65	8.94	9.10	0	2.26
ML&(Acc Cat Don)	F5	3.64	9.49	9.49	2.26	0

$$\text{Sensitivity} = \frac{\text{True positive}}{\text{True positive} + \text{False negative}}$$

$$\text{Sensitivity} = \frac{50}{50 + 13}$$

$$\text{Sensitivity} = \frac{50}{50 + 13}$$

$$\text{Sensitivity} = 79\%$$

The model has 79% sensitivity to distinguishing between active and inactive test compounds.

$$\text{Spifecicity} = \frac{\textit{True negative}}{\textit{True negative} + \textit{False positive}}$$

$$\text{Specificity} = \frac{156}{156 + 44}$$

$$\text{Spifecicity} = \frac{\textit{True negative}}{\textit{True negative} + \textit{False positive}}$$

$$\text{Specificity} = \frac{156}{156 + 44}$$

$$\text{Specificity} = 78\%$$

The model has 78% specificity towards active compounds as hits.

The overall calculated results provide an understanding of the ligands binding to uPA receptor protein by mapping the binding domains, also given the mutual distances between the selected pharmacophoric features that include four cationic hydrogen bond acceptors, two hydrogen bond donors and a hydrophobic aromatic ring.

4.4 Quantum mechanical studies

4.4.1 Model extraction

The ligand protein complex of uPA with its ligand SR3 obtained as a result through docking using GOLD software was further utilised for quantum mechanical studies. It is not computationally feasible to perform Density functional studies on the complete protein as it is very costly and would take a lot of time in calculating results. Therefore, the amino acid residues in close vicinity to the ligand (SR3) were extracted for further evaluation using a free protein homology modelling server Swiss-Pdb (SPDB) Viewer. For quantum mechanical studies, the protein ligand complex needs to be truncated and reduced to the level of only ligand and the amino acid residues, ASP189, GLY216, GLY219, SER190, SER214, HIS57, TRP215 and LYS224 in the target protein located at the binding site and takes part in the binding interactions. The extracted model is given below in Figure 4.21.

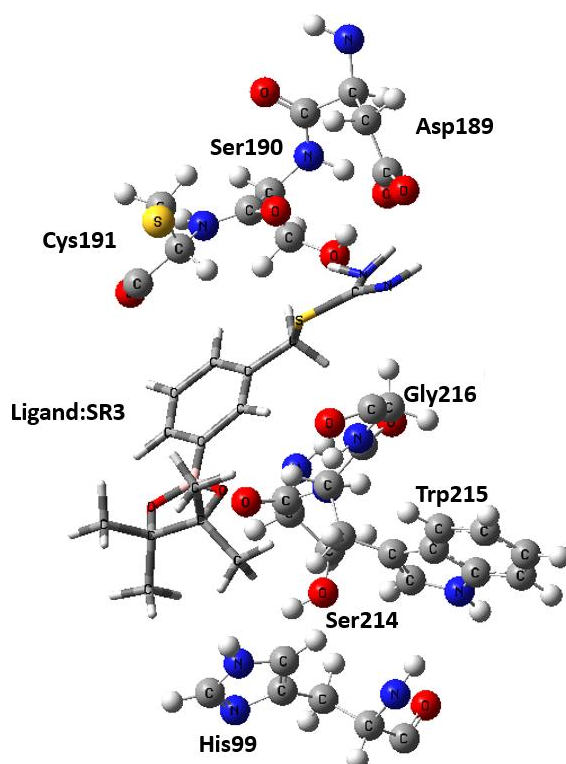


Figure 4.21 Selected residues of the binding pocket of uPA with its bound ligand extracted using SPDB viewer. The tube represents the ligand SR3 and the ball and stick model represent the amino acid residues of the binding pocket. For simplicity and clear visualise

4.4.2 Ligand-protein complex geometry optimization

The extracted model of the binding pocket with bound ligand SR3 was passed through a series of clippings and modifications by trimming the amino acid residues ASP189, HIS99, SER214 and TRP215 at their alpha carbon (α -carbon) atom positions. To satisfy the valency where the cuttings were made, hydrogen atoms were added to the carbons of HIS99, SER214 and TRP215. Figure 4.22 given below depicts the selected binding pocket in complex with ligand SR3 with the needed clippings and modifications.

The modified complex geometry of the product designed was subjected to optimization. The first step was hydrogen optimization where all the atoms except hydrogen were fixed. Once the hydrogens were optimized, this optimized geometry is then subjected to the next step that is geometry optimization of the model complex. During geometry optimization some of the atoms at the alpha carbons of amino acid residues ASP189, HIS99, SER214 and TRP215 are fixed, throughout the quantum mechanical studies being carried out, at

Results and Discussion

locations where the trimmings were made so that they would stay on their positions of the X-ray crystal structure and retain the effect of normal protein.

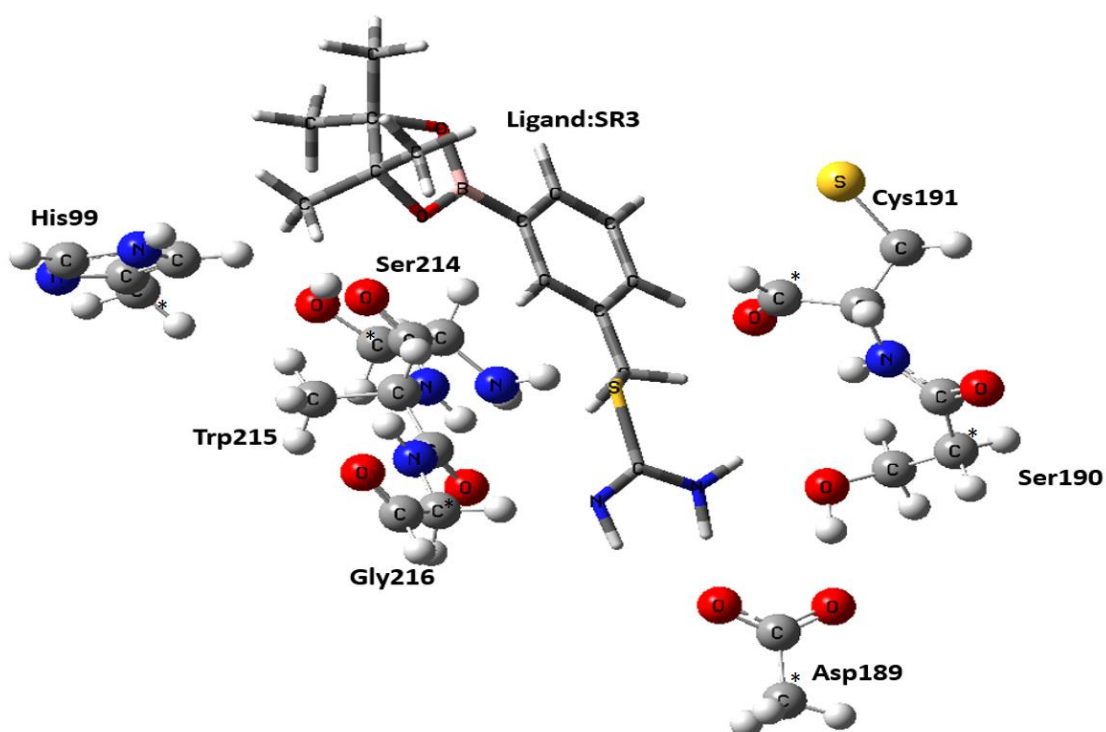


Figure 4.22 Proposed optimized model complex of uPA binding pocket with ligand SR3. The sticks represent the ligand SR3 while the ball and lines represent the amino acid residues of the binding site. Asterics represent the fixed carbons where the cuttings are made.

For geometry optimization hybrid density functional method B3LYP was used in combination with a basis set LANL2DZ. The optimized geometry was then further utilised in the calculation of the single point energies in both gas and solvent phase using B3LYP/LANL2DZ level of DFT.

4.4.3 Binding pocket geometry optimization

To understand the protein binding interaction energy, the optimized geometry of protein-ligand complex were used. To obtain minimized energy for protein binding pocket without ligand, ligand structure was removed and then protein binding pocket geometry model was optimized using same level of DFT, B3LYP/LANL2DZ. Figure 4.23 given below depicts the selected binding pocket without the ligand.

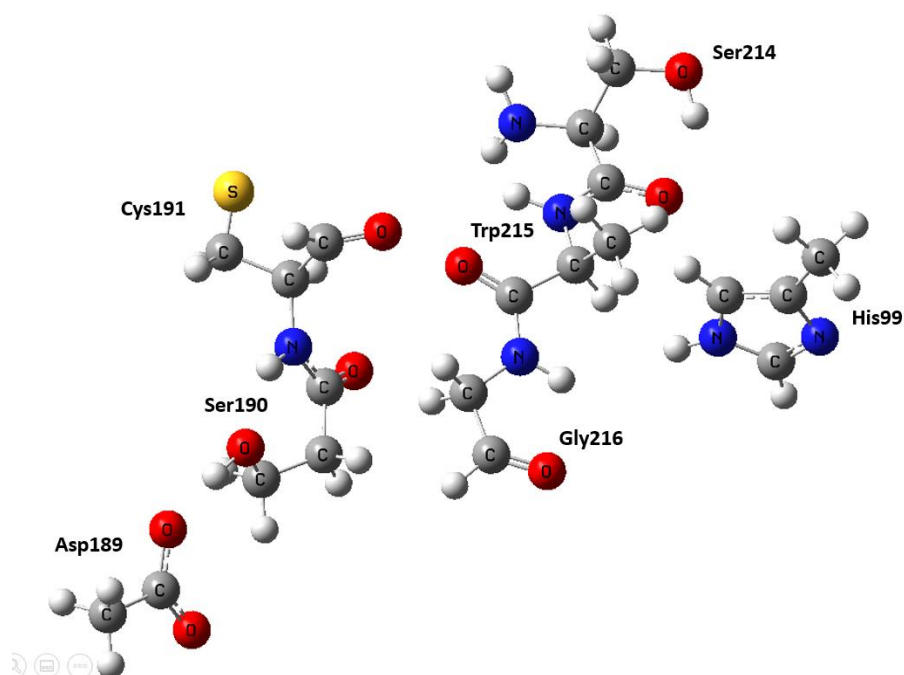


Figure 4.23 The optimized binding pocket of uPA

4.4.4 Ligand Geometry optimization

For ligand model geometry optimization, ligand SR3 was extracted from X-ray crystal structure, PDB ID: 1W10 [86]. Figure 4.24 shows the image of optimized ligand SR3 which was optimized using B3LYP/LANL2DZ level of DFT studies.

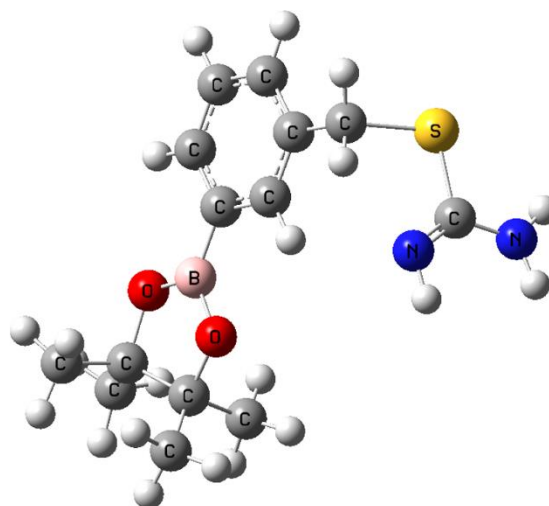


Figure 4.24 Optimized geometry of ligand SR3

4.4.5 Frequency calculation for all optimized geometries

To ensure that all the model geometries are fully optimized, frequency calculations were performed on the optimized ligand, protein, and protein-ligand complex using DFT method (B3LYP/LANL2DZ). Result shows that there is no imaginary frequency present in all three model geometries and hence they are the energy minimised structures.

4.4.6 Single point energy calculation for all optimized geometries

Single point energies were calculated on all the optimized geometries in both gas phase as well as in solvent phase. As biological systems are surrounded by solvents and fluids, we consider water as the solvent. The ligand and protein molecules acting as solute present within the solvent polarise in response to the solvent polarisation. And conversely the molecules of the solvent rearrange themselves and polarise in response to the charge density of the solute. This polarisation induces redistribution of charges between the solute and the solvent until they reach a state of self-consistency which lowers the energy of the whole system and stabilises it.

Ligand Binding Affinity

The ligand binding affinity for ligand SR3 with protein uPA was calculated using Equation 4.1 given below

$$\Delta G_{bind} = G_{complex} - G_{receptor} - G_{ligand}. \quad (4.2)$$

Where

ΔG_{bind} is the ligand binding affinity

$G_{complex}$ is the energy of the ligand bound to the binding pocket

$G_{receptor}$ is the energy calculated for the binding pocket

G_{ligand} is the energy calculated for optimized ligand

Results and Discussion

All these G values are calculated in a.m.u (atomic mass unit), therefore, to convert it to kcal/mol, it needs to be multiplied with 627.51. Therefore, the equation 4.1 can also be written as follows:

$$\Delta G_{bind} = 627.51 (G_{complex} - G_{receptor} - G_{ligand}) \quad (4.2)$$

The computed relative energy value (Kcal/mol) for binding affinity of SR3 is presented in the Table 4.6 given below

Table 4.6 Computed energies in kcal/mol for optimized geometry, Single point energy and self-consistent reaction field for Sr3 bound uPA binding cavity with the methods used as level of DFT

	Relative energy (kcal/mol)	Level of DFT
OPT	53.9	B3LYP/LANL2DZ
SPE	-66.3	B3LYP/LANL2DZ// B3LYP/LANL2DZ
SCRF	-49.0	CPCM-B3LYP/LANL2DZ(p)//B3LYP/LANL2DZ

The results indicate that the binding interaction between SR3 and uPA is stable/feasible as the relative energy is exothermic with the release of -49.0 kcal/mol energy.

5 Conclusion

Knowing up to date computational quantum mechanical techniques are unable to produce very accurate results for the binding free energies specifically in case of ligand and proteins in solvent environment that mimic the real situation. Consequently, the quantum mechanical techniques would be appropriate for the prediction purposes instead of the precise estimation of binding free energies for the ligands and proteins. The development of inhibitors containing moieties which can interact with different uPA sub-sites with high selectivity, potency, and improved pharmacokinetic properties are the main challenges at this stage. It is hoped that the results presented here should stimulate combining experimental and theoretical works for developing uPA inhibitors in cancer treatment through a better understanding of the binding interaction of uPA and its inhibitors.

Structure based technique molecular docking was used to produce a protocol for validation of the previously present binding interactions between seven ligands (BC11, BC57, SR3, JS62, JS67, AB11 and AB4/5) and uPA and ligand based techniques were combined with them for demonstrating the importance of significant descriptors for optimum biological activity at receptor site by the inhibitor. Molecular docking simulations were performed to hypothesise the binding activity with the help two software. The results generated were analysed not only based on calculated score, but the residues involved in the binding as well. Ligand SR3 was chosen as most suitable inhibitor among seven with score -3.2481 kcal/mol with MOE and 46.4523 kcal/mol with GOLD. SR3 showed interactions with receptor amino acid residues GLY219, SER190 and ASP189 with Sulphur and amino group generated by MOE and GLY219, GLY216, ASP189 with Sulphur, amine and amino group generated by GOLD. A pharmacophore model was designed because of significant descriptors. These descriptors can be used to search for compounds that may act as efficient inhibitors that fit the model. As these features are characterised as essential regarding the biological activity of inhibitors against uPA.

Conclusion

The biological activity was correlated with effect of 3 dimensional (3D) properties of ligands. It was concluded from the results of QSAR that in uPA two hydrogen bond donor groups at distance of 2.2 Å apart were considered a favourable for activity. There is an aromatic hydrophobic ring at a distance of 5.95 Å and 5.85 Å from the two hydrogen bond donor groups and at a distance of 3.65 Å and 3.64 Å from the two metal ligator hydrogen bond acceptor groups. Also, the two metal ligator hydrogen bond acceptor groups are situated at 2.2 Å apart from each other. The designed model shows 79% Sensitivity, 78% Specificity and 51% calculated MCC. This model was tested for a test set of 263 boronic acid derived inhibitors against uPA to predict the accountability of the model by judging how well it can differentiate between active and inactive compounds with a specific activity cut-off. This model can further be tested for liability through experimental methods.

Computational Quantum mechanical studies were applied based upon the electron density of uPA to find the binding energy of active ligand against receptor uPA using hybrid functional B3LYP in combination with LANL2DZ of Density Functional Theory (DFT) as basis set on the selected model of active site of uPA. A -2 charge is present on ASP189 of the binding cavity throughout the simulations. From the computational analysis of the calculated values

Geometric optimization (opt) = 53.9

Single point energy (SPE) = -66.3

Self-consistent reaction field (SCRF) = -49.0

It is concluded that uPA shows better binding with ligand when there is a negative two charge on it ASP189 amino acid residue in the binding pocket.

5.1 References

- [1] World Health Organisation, *GUIDE TO CANCER Guide to cancer early diagnosis*. 2017.
- [2] A. Αρβανίτη, Α. Σπυροπούλου, and Ι. Ζέρβας, “Ειδικό άρθρο Special article,” vol. 23, no. 4, pp. 314–321, 2012.
- [3] X. Guan, “Cancer metastases: challenges and opportunities.,” *Acta Pharm. Sin. B*, vol. 5, no. 5, pp. 402–18, 2015.
- [4] P. A. Andreasen, L. Kjøller, L. Christensen, and M. J. Duffy, “The urokinase-type plasminogen activator system in cancer metastasis: A review - Andreasen - 1998 - International Journal of Cancer - Wiley Online Library,” *Int. J. Cancer*, vol. 72, no. 1, pp. 1–22, 1997.
- [5] M. Wang *et al.*, “Role of tumor microenvironment in tumorigenesis,” *J. Cancer*, vol. 8, no. 5, pp. 761–773, 2017.
- [6] R. Smoum, A. Rubinstein, V. M. Dembitsky, and M. Srebnik, “Boron Containing Compounds as Protease Inhibitors,” *Chem. Rev.*, vol. 112, no. 7, pp. 4156–4220, 2012.
- [7] E. Di Cera, “Serine Proteases Enrico,” *Int. Union Biochem. Mol. Biol. Life*, vol. 61, no. 5, pp. 510–515, 2009.
- [8] C. López-Otín and J. S. Bond, “Proteases: Multifunctional Enzymes in Life and Disease,” *J. Biol. Chem.*, vol. 283, no. 45, pp. 30433–30437, 2008.
- [9] D. Brungs *et al.*, “The urokinase plasminogen activation system in gastroesophageal cancer: A systematic review and meta-analysis,” *Oncotarget*, vol. 8, no. 14, pp. 23099–23109, 2017.
- [10] S. Barberi, G. Montagna, and L. Rossi, “Expression of urokinase plasminogen activator (uPA) in the leukocytes and tissues of patients with benign and malignant breast lesions,” *Breast Dis.*, vol. 38, no. 1, pp. 15–23, 2019.
- [11] L. H. Dohn *et al.*, “Urokinase-type plasminogen activator receptor (uPAR) expression is associated with T-stage and survival in urothelial carcinoma of the bladder,” *Urol. Oncol. Semin. Orig. Investig.*, vol. 33, no. 4, p. 165.e15-165.e24, 2015.

References

- [12] C. Borgfeldt, S. R. Hansson, B. Gustavsson, A. Måsbäck, and B. Casslén, “Dedifferentiation of serous ovarian cancer from cystic to solid tumors is associated with increased expression of mRNA for urokinase plasminogen activator (uPA), its receptor (uPAR) and its inhibitor (PAI-1),” *Int. J. Cancer*, vol. 92, no. 4, pp. 497–502, 2001.
- [13] N. Mahmood, C. Mihalcioiu, and S. A. Rabbani, “Multifaceted Role of the Urokinase-Type Plasminogen Activator (uPA) and Its Receptor (uPAR): Diagnostic, Prognostic, and Therapeutic Applications,” *Front. Oncol.*, vol. 8, no. February, 2018.
- [14] N. Montuori *et al.*, “Urokinase type plasminogen activator receptor (uPAR) as a new therapeutic target in cancer,” vol. 15, no. 3, pp. 15–21, 2016.
- [15] Z. J. Leśnikowski, “Challenges and Opportunities for the Application of Boron Clusters in Drug Design,” *J. Med. Chem.*, vol. 59, no. 17, pp. 7738–7758, 2016.
- [16] D. B. Diaz and A. K. Yudin, “The versatility of boron in biological target engagement,” *Nat. Chem.*, vol. 9, no. 8, pp. 731–742, 2017.
- [17] D. G. Hall, “Boronic Acids: Preparation and Applications in Organic Synthesis, Medicine and Materials (Volume 1 and 2),” *Boronic Acids Prep. Appl. Org. Synth. Med. Mater. (Volume 1 2)*, vol. 1–2, 2011.
- [18] P. C. Trippier and C. McGuigan, “Boronic acids in medicinal chemistry: Anticancer, antibacterial and antiviral applications,” *Medchemcomm*, vol. 1, no. 3, pp. 183–198, 2010.
- [19] W. L. A. Brooks and B. S. Sumerlin, “Synthesis and Applications of Boronic Acid-Containing Polymers: From Materials to Medicine,” *Chem. Rev.*, vol. 116, no. 3, pp. 1375–1397, 2016.
- [20] J. P. M. António, R. Russo, C. P. Carvalho, P. M. S. D. Cal, and P. M. P. Gois, “Boronic acids as building blocks for the construction of therapeutically useful bioconjugates,” *Chem. Soc. Rev.*, vol. 48, no. 13, pp. 3513–3536, 2019.
- [21] J. P. Hughes, S. S. Rees, S. B. Kalindjian, and K. L. Philpott, “Principles of early drug discovery,” *Br. J. Pharmacol.*, vol. 162, no. 6, pp. 1239–1249, 2011.
- [22] C. A. Lipinski, F. Lombardo, B. W. Dominy, and P. J. Feeney, “Experimental and computational approaches to estimate solubility and permeability in drug discovery and development settings,” *Adv. Drug Deliv. Rev.*, vol. 64, no. SUPPL., pp. 4–17, 2012.
- [23] H. Maesaka, K. Fukazawa, S. Suwa, and A. Goto, “Case of diabetes insipidus with

References

- thyroxine binding globulin deficiency,” *Hormon To Rinsho.*, vol. 26, no. 11, pp. 1208–1213, 1978.
- [24] J. Weigelt, “Structural genomics-Impact on biomedicine and drug discovery,” *Exp. Cell Res.*, vol. 316, no. 8, pp. 1332–1338, 2010.
- [25] L. G. Ferreira, R. N. Dos Santos, G. Oliva, and A. D. Andricopulo, *Molecular docking and structure-based drug design strategies*, vol. 20, no. 7. 2015.
- [26] M. Wilmes and H. Sahl, “Chapter 8 Determination of Bacterial Membrane Impairment,” vol. 1520, pp. 133–143, 2018.
- [27] C. H. Lee, H. C. Huang, and H. F. Juan, “Reviewing ligand-based rational drug design: The search for an ATP synthase inhibitor,” *Int. J. Mol. Sci.*, vol. 12, no. 8, pp. 5304–5318, 2011.
- [28] T. Kaserer, K. R. Beck, M. Akram, A. Odermatt, D. Schuster, and P. Willett, “Pharmacophore models and pharmacophore-based virtual screening: Concepts and applications exemplified on hydroxysteroid dehydrogenases,” *Molecules*, vol. 20, no. 12, pp. 22799–22832, 2015.
- [29] R. A. Friesner, “Ab initio quantum chemistry: Methodology and applications,” *Proc. Natl. Acad. Sci. U. S. A.*, vol. 102, no. 19, pp. 6648–6653, 2005.
- [30] E. M. Papamichael, H. Stamatis, P.-Y. Stergiou, A. Foukis, and O. A. Gkini, *Enzyme Kinetics and Modeling of Enzymatic Systems*. Elsevier B.V., 2019.
- [31] P. G. Mezey and P. D. Walker, “Fuzzy molecular fragments in drug research,” *Drug Discov. Today*, vol. 2, no. 4, pp. 132–137, 1997.
- [32] H. Tandon, T. Chakraborty, and V. Suhag, “A Brief Review on Importance of DFT In Drug Design,” pp. 791–795, 2019.
- [33] S. LaPointe and D. Weaver, “A Review of Density Functional Theory Quantum Mechanics as Applied to Pharmaceutically Relevant Systems,” *Curr. Comput. Aided-Drug Des.*, vol. 3, no. 4, pp. 290–296, 2007.
- [34] K. Capelle, “A Bird’s-Eye View of Density-Functional Theory,” vol. 36, no. 4, pp. 1318–1343, 2006.
- [35] O. A. Arodola and M. E. S. Soliman, “Quantum mechanics implementation in drug-design workflows: Does it really help?,” *Drug Des. Devel. Ther.*, vol. 11, pp. 2551–2564, 2017.
- [36] J.-K. Hsiao, B. Law, R. Weissleder, and C.-H. Tung, “In-vivo imaging of tumor

References

- associated urokinase-type plasminogen activator activity,” *J. Biomed. Opt.*, vol. 11, no. 3, p. 034013, 2006.
- [37] J. Dang, Y. Wang, and W. F. Doe, “Sodium butyrate inhibits expression of urokinase and its receptor mRNAs at both transcription and post-transcription levels in colon cancer cells,” *FEBS Lett.*, vol. 359, no. 2–3, pp. 147–150, 1995.
- [38] C. Y. Li, S. J. de Veer, R. H. P. Law, J. C. Whisstock, D. J. Craik, and J. E. Swedberg, “Characterising the Subsite Specificity of Urokinase-Type Plasminogen Activator and Tissue-Type Plasminogen Activator using a Sequence-Defined Peptide Aldehyde Library,” *ChemBioChem*, vol. 20, no. 1, pp. 46–50, 2019.
- [39] B. Weigelt, J. L. Peterse, and L. J. Van’t Veer, “Breast cancer metastasis: Markers and models,” *Nat. Rev. Cancer*, vol. 5, no. 8, pp. 591–602, 2005.
- [40] A. Schweinitz *et al.*, “Design of novel and selective inhibitors of urokinase-type plasminogen activator with improved pharmacokinetic properties for use as antimetastatic agents,” *J. Biol. Chem.*, vol. 279, no. 32, pp. 33613–33622, 2004.
- [41] K. Almholt *et al.*, “Reduced metastasis of transgenic mammary cancer in urokinase-deficient mice,” *Int. J. Cancer*, vol. 113, no. 4, pp. 525–532, 2005.
- [42] N. Ahmed, K. Oliva, Y. Wang, M. Quinn, and G. Rice, “Downregulation of urokinase plasminogen activator receptor expression inhibits Erk signalling with concomitant suppression of invasiveness due to loss of uPAR- β 1 integrin complex in colon cancer cells,” *Br. J. Cancer*, vol. 89, no. 2, pp. 374–384, 2003.
- [43] S. D’Alessio *et al.*, “Antisense oligodeoxynucleotides for urokinase-plasminogen activator receptor have anti-invasive and anti-proliferative effects in vitro and inhibit spontaneous metastases of human melanoma in mice,” *Int. J. Cancer*, vol. 110, no. 1, pp. 125–133, 2004.
- [44] C. Ostheimer, C. Evers, M. Bache, T. Reese, and D. Vordermark, “Prognostic implications of the co-detection of the urokinase plasminogen activator system and osteopontin in patients with non-small-cell lung cancer undergoing radiotherapy and correlation with gross tumor volume,” *Strahlentherapie und Onkol.*, vol. 194, no. 6, pp. 539–551, 2018.
- [45] J. F. Santibanez, “Transforming Growth Factor-Beta and Urokinase-Type Plasminogen Activator: Dangerous Partners in Tumorigenesis-Implications in Skin Cancer,” *ISRN Dermatology Vol. 2013, Artic. ID 597927, 26 pages*, vol. 2013, pp. 1–27, 2014.
- [46] K. H. Lee, E. Y. Choi, M. S. Hyun, and J. R. Kim, “Involvement of MAPK pathway in hypoxia-induced up-regulation of urokinase plasminogen activator receptor in a

References

- human prostatic cancer cell line, PC3MLN4,” *Exp. Mol. Med.*, vol. 36, no. 1, pp. 57–64, 2004.
- [47] “Department of Biological Sciences and Institute for Biomolecular Sciences, University of Wollongong, Australia, 2522 and The Scripps Research Institute, La Jolla, CA, USA, CVN-26,” no. 17, 2003.
- [48] J. A. Aguirre Ghiso, D. F. Alonso, E. F. Farias, D. E. Gomez, and E. Bal De Kier Joffè, “Deregulation of the signaling pathways controlling urokinase production: Its relationship with the invasive phenotype,” *Eur. J. Biochem.*, vol. 263, no. 2, pp. 295–304, 1999.
- [49] C.-W. Lin, S.-F. Yang, W.-E. Yang, W.-L. Fan, and S.-C. Su, “The urokinase-type plasminogen activator (uPA) system as a biomarker and therapeutic target in human malignancies,” *Expert Opin. Ther. Targets*, vol. 20, no. 5, pp. 551–566, 2015.
- [50] P. Lu, K. Takai, V. M. Weaver, and Z. Werb, “Extracellular Matrix degradation and remodeling in development and disease,” *Cold Spring Harb. Perspect. Biol.*, vol. 3, no. 12, pp. 1–24, 2011.
- [51] T. R. Cox and J. T. Eler, “Remodeling and homeostasis of the extracellular matrix: Implications for fibrotic diseases and cancer,” *DMM Dis. Model. Mech.*, vol. 4, no. 2, pp. 165–178, 2011.
- [52] K. R. Levental *et al.*, “Matrix Crosslinking Forces Tumor Progression by Enhancing Integrin Signaling,” *Cell*, vol. 139, no. 5, pp. 891–906, 2009.
- [53] S. S. Mali, A. V., Joshi, A. A., Hegde, M. V., Kadam, “Enterolactone Suppresses Proliferation, Migration and Metastasis of MDA-MB-231 Breast Cancer Cells Through Inhibition of uPA Induced Plasmin Activation and MMPs-Mediated ECM Remodeling,” *Asian Pacific J. Cancer Prev.*, vol. 18, no. 4, pp. 905–915, 2017.
- [54] D. Cantero *et al.*, “Enhanced expression of urokinase plasminogen activator and its receptor in pancreatic carcinoma,” *Br. J. Cancer*, vol. 75, no. 3, pp. 388–395, 1997.
- [55] J. Adams and M. Kauffman, “Development of the proteasome inhibitor Velcade™ (Bortezomib),” *Cancer Invest.*, vol. 22, no. 2, pp. 304–311, 2004.
- [56] C. G. Neochoritis *et al.*, “Rapid approach to complex boronic acids,” no. July, pp. 1–9, 2019.
- [57] J. ADAMS *et al.*, “ChemInform Abstract: Potent and Selective Inhibitors of the Proteasome: Dipeptidyl Boronic Acids,” *ChemInform*, vol. 29, no. 21, p. no-no, 2010.

References

- [58] G. Xue *et al.*, “A structural mechanism of flavonoids in inhibiting serine proteases,” *Food Funct.*, vol. 8, no. 7, pp. 2437–2443, 2017.
- [59] D. Hutchison and J. C. Mitchell, *Lecture Notes in Computer Science*, vol. 9, no. 3, 1973.
- [60] R. S. Bohacek, C. McMartin, and W. C. Guida, “The art and practice of structure-based drug design: A molecular modeling perspective,” *Med. Res. Rev.*, vol. 16, no. 1, pp. 3–50, 1996.
- [61] M. D. Corte *et al.*, “Tissue-Type plasminogen activator (tPA) in breast cancer: Relationship with clinicopathological parameters and prognostic significance,” *Breast Cancer Res. Treat.*, vol. 90, no. 1, pp. 33–40, 2005.
- [62] I. K. Lund, M. Illemann, T. Thurison, I. J. Christensen, and G. Hoyer-Hansen, “uPAR as Anti-Cancer Target: Evaluation of Biomarker Potential, Histological Localization, and Antibody-Based Therapy,” *Curr. Drug Targets*, vol. 12, no. 12, pp. 1744–1760, 2011.
- [63] J. Tyndall, M. Kelso, P. Clingan, and M. Ranson, “Peptides and Small Molecules Targeting the Plasminogen Activation System: Towards Prophylactic Anti-Metastasis Drugs for Breast Cancer,” *Recent Pat. Anticancer. Drug Discov.*, vol. 3, no. 1, pp. 1–13, 2008.
- [64] V. B. Sulimov *et al.*, “Application of molecular modeling to urokinase inhibitors development,” *Biomed Res. Int.*, vol. 2014, 2014.
- [65] L. B. Salum, I. Polikarpov, and A. D. Andricopulo, “Structure-based approach for the study of estrogen receptor binding affinity and subtype selectivity,” *J. Chem. Inf. Model.*, vol. 48, no. 11, pp. 2243–2253, 2008.
- [66] “CHAPTER 3 Pharmacophore modelling studies : Introduction :,” no. 2004, pp. 54–89, 2010.
- [67] M. A. Al-Sha’er, M. A. Khanfar, and M. O. Taha, “Discovery of novel urokinase plasminogen activator (uPA) inhibitors using ligand-based modeling and virtual screening followed by in vitro analysis,” *J. Mol. Model.*, vol. 20, no. 1, 2014.
- [68] M. D. Wendt *et al.*, “Interaction with the S1 β -pocket of urokinase: 8-heterocycle substituted and 6,8-disubstituted 2-naphthamidine urokinase inhibitors,” *Bioorganic Med. Chem. Lett.*, vol. 14, no. 12, pp. 3063–3068, 2004.
- [69] C. Solis-Calero, G. Zanatta, C. do Ó. Pessoa, H. F. Carvalho, and V. N. Freire, “Explaining urokinase type plasminogen activator inhibition by amino-5-hydroxybenzimidazole and two naphthamidine-based compounds through quantum

References

- biochemistry,” *Phys. Chem. Chem. Phys.*, vol. 20, no. 35, pp. 22818–22830, 2018.
- [70] A. Volkamer, D. Kuhn, F. Rippmann, and M. Rarey, “Dogsitescorer: A web server for automatic binding site prediction, analysis and druggability assessment,” *Bioinformatics*, vol. 28, no. 15, pp. 2074–2075, 2012.
- [71] G. Náray-Szabó, A. Perczel, A. Láng, and D. K. Menyhárd, “Protein modeling,” *Handb. Comput. Chem.*, vol. 79, no. Suppl 10, pp. 1589–1626, 2017.
- [72] V. Hornak, R. Abel, A. Okur, B. Strockbine, A. Roitberg, and C. Simmerling, “Comparison of multiple amber force fields and development of improved protein backbone parameters,” *Proteins Struct. Funct. Genet.*, vol. 65, no. 3, pp. 712–725, 2006.
- [73] S. Vilar, G. Cozza, and S. Moro, “Medicinal chemistry and the molecular operating environment (MOE): application of QSAR and molecular docking to drug discovery,” *Curr. Top. Med. Chem.*, vol. 8, no. 18, pp. 1555–72, 2008.
- [74] J. Ervø *et al.*, “Giftgas over Byen. Civilbefolkningens Beskyttelse Under Den Næste krig,” vol. 623, no. January, pp. 609–623, 1933.
- [75] T. Schwede, J. Kopp, N. Guex, and M. C. Peitsch, “SWISS-MODEL: An automated protein homology-modeling server,” *Nucleic Acids Res.*, vol. 31, no. 13, pp. 3381–3385, 2003.
- [76] T. Zhou, D. Huang, and A. Caflisch, “Quantum Mechanical Methods for Drug Design,” *Curr. Top. Med. Chem.*, vol. 10, no. 1, pp. 33–45, 2010.
- [77] S. J. Fox, J. Dziedzic, T. Fox, C. S. Tautermann, and C. K. Skylaris, “Density functional theory calculations on entire proteins for free energies of binding: Application to a model polar binding site,” *Proteins Struct. Funct. Bioinforma.*, vol. 82, no. 12, pp. 3335–3346, 2014.
- [78] B. F. Ion, E. A. C. Bushnell, P. De Luna, and J. W. Gault, “A molecular dynamics (MD) and quantum mechanics/molecular mechanics (QM/MM) study on ornithine cyclodeaminase (OCD): A tale of two iminiums,” *Int. J. Mol. Sci.*, vol. 13, no. 10, pp. 12994–13011, 2012.
- [79] X. Yang, S. Wang, and X. Ma, “Application of microwave technique in the preparation of catalyst,” *Chem. Bull. / Huaxue Tongbao*, vol. 67, no. 9, pp. 641–647, 2004.
- [80] Cooper, “No 主観的健康感を中心とした在宅高齢者における 健康関連指標に関する共分散構造分析Title,” pp. 5–10, 2019.

References

- [81] M. Girod and B. Grammaticos, “The zero-point energy correction and its effect on nuclear dynamics,” *Nucl. Physics, Sect. A*, vol. 330, no. 1, pp. 40–52, 1979.
- [82] J. M. L. Martin and A. Sundermann, “Correlation consistent valence basis sets for use with the Stuttgart-Dresden-Bonn relativistic effective core potentials: the atoms Ga-Kr and In-Xe,” *J. Chem. Phys.*, vol. 114, no. 8, pp. 3408–3420, 2001.
- [83] G. Kahl, “Molecular docking,” *Dict. Genomics, Transcr. Proteomics*, vol. 443, pp. 1–1, 2015.
- [84] T. Rockway, V. Nienaber, and V. Giranda, “Inhibitors of the Protease Domain of Urokinase-Type Plasminogen Activator,” *Curr. Pharm. Des.*, vol. 8, no. 28, pp. 2541–2558, 2005.
- [85] H. A. Hussein, A. Borrel, C. Geneix, M. Petitjean, L. Regad, and A. C. Camproux, “PockDrug-Server: A new web server for predicting pocket druggability on holo and apo proteins,” *Nucleic Acids Res.*, vol. 43, no. W1, pp. W436–W442, 2015.
- [86] E. Zeslawska, U. Jacob, A. Schweinitz, G. Coombs, W. Bode, and E. Madison, “Crystals of urokinase type plasminogen activator complexes reveal the binding mode of peptidomimetic inhibitors,” *J. Mol. Biol.*, vol. 328, no. 1, pp. 109–118, 2003.